Supporting Information

Highly-soluble multi-alkylated polymer semiconductors and applications in high-performance field-effect transistors

Zhihui Chen, Jianyao Huang, Dong Gao, Jie Yang, Weifeng Zhang, Huanxin Ju, and Gui Yu*

Supporting Information

Highly-soluble multi-alkylated polymer semiconductors and applications in high-performance field-effect transistors

Zhihui Chen, Jianyao Huang, Dong Gao, Jie Yang, Weifeng Zhang, Huanxin Ju, and Gui Yu[*]

Corresponding Author
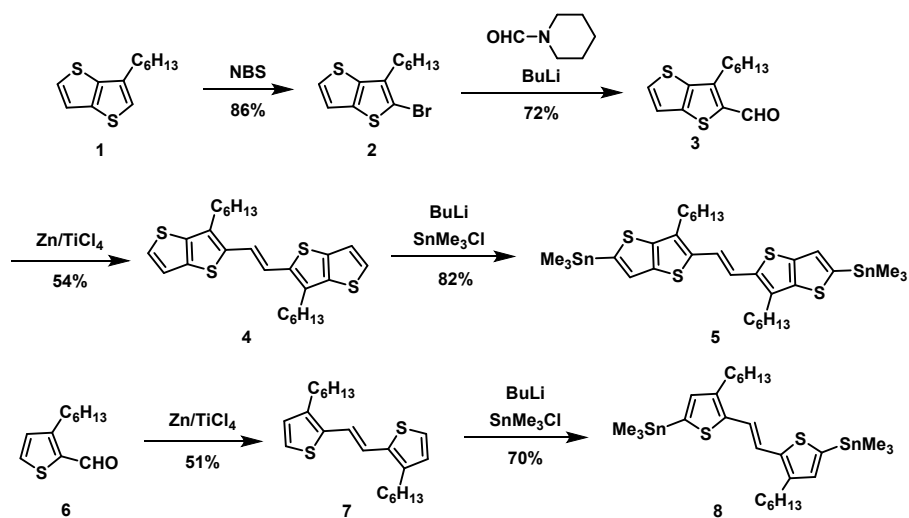
*yugui@iccas.ac.cn

Content

1. Synthetic procedure and NMR spectra of new compounds

The chemical reagents were purchased from Alfa, Acros, and J&K chemical without further purification. If necessary, the anhydrous solvents were purified by following standard procedures.

^{1}H NMR and ^{13}C NMR spectra of the small molecules were recorded on a Bruker Avance 300 MHz spectrometer. The ^{1}H NMR spectra of the polymers were recorded on a Bruker Avance 300 MHz spectrometer at 373K. Gel–permeation chromatography (GPC) was performed on an Agilent PL-GPC 220 using polystyrene as a standard with the eluent of 1,2,4-trichlorobenzene. Ultraviolet photoelectron spectroscopy (UPS) was examined by Axis-Nova CJ109, Kratos with a photoelectron energy of 21.22 eV. Cyclic voltammetry (CV) experiments were conducted with a structure of three-electrode cell on the electrochemistry workstation (CHI660c, Chenhua Shanghai), in which a Ag/AgCl (Ag in a 0.01 mol L^{-1} KCl) electrode was used as the reference electrode and a platinum wire as the counter electrode. A platinum stick electrode coated with a thin film layer of polymer was used as the working electrode. Anhydrous solution of 0.1 M tetrabutylammonium hexafluorophosphate in acetonitrile was employed as the electrolyte. Before testing, nitrogen was bubbled into the solution. The energy levels were calibrated using Fc$^+$/Fc (-4.80 eV). The HOMO and LUMO energy levels were calculated from onset of the corresponding peaks by using the equations $E_{\text{HOMO}} = -(E_{\text{ox,onset}} + 4.40)$ eV and

$E_{\text{LUMO}} = -(E_{\text{re,onset}} + 4.40)$ eV. UV–vis absorption spectra were measured using a J-570 spectrometer. The morphology of the polymer thin films was imaged under ambient condition using a Digital Instruments Nanoscope V atomic force microscope operated in tapping mode, which were identical to those characterized in the respective OFETs. Raman spectra were recorded using LabRAM HR Evolution with laser excitation at 633 nm. Carbon K-edge near-edge X-ray absorption fine structure (NEXAFS) spectroscopy was performed on a Soft X-ray Magnetic Circular Dichroism Endstation (SXMCD) in total electron yield (TEY) mode at National Synchrotron Radiation Laboratory (NSRL) in Hefei, China. The NEXAFS spectra were fitted with Gaussian functions in conjunction with a step function background subtraction.

Scheme S1 Synthesis of monomers.

**Scheme S2** Synthetic routes to four polymers.

M1 =

M2 =

M1 + M2 → Pd₂(dba)₃/P(o-tol)₃

PD-10-TVT-6

PBD-10-TVT-6

PD-10-DTTE-6

PBD-10-DTTE-6
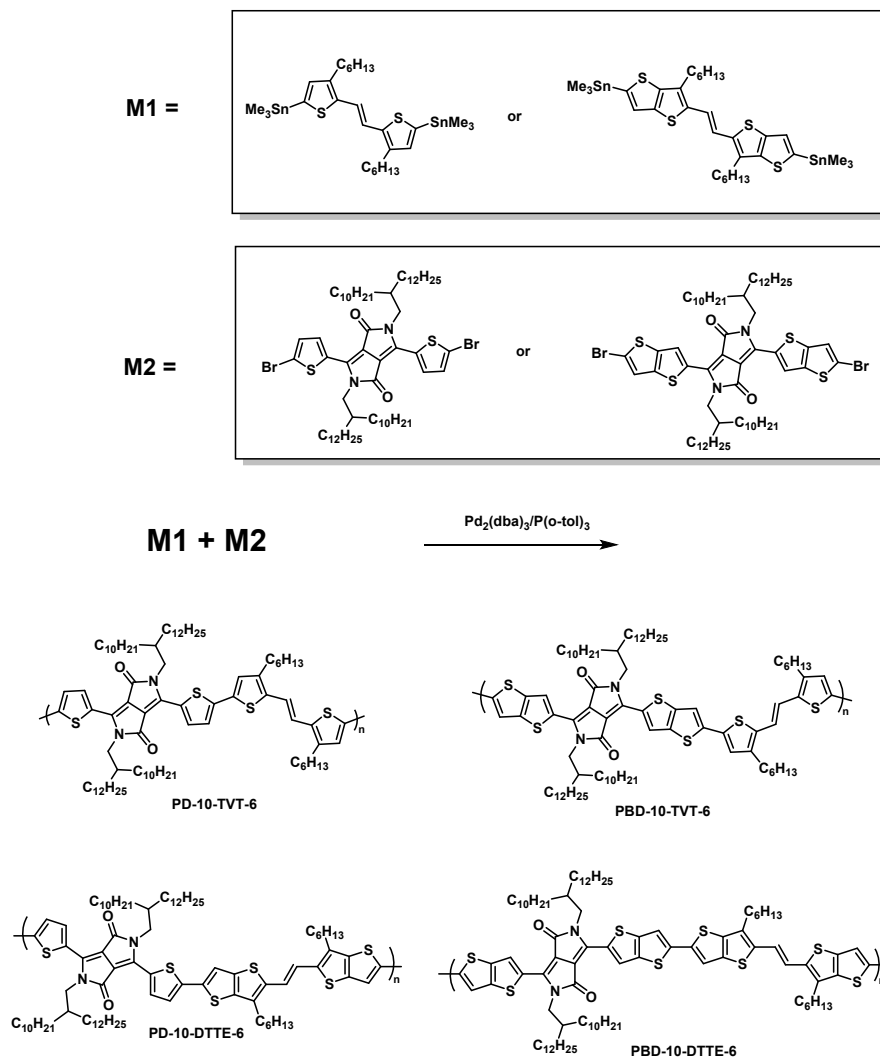
3-Hexylthieno[3,2-*b*]thiophene (Compound 1) was synthesized by following the literature methods.[1]

^{1}H NMR (300 MHz, CD$_2$Cl$_2$, δ): 7.40 (dd, *J* = 5.2, 1.6 Hz, 1H), 7.27 (d, *J* = 5.2 Hz, 1H), 7.03 (d, *J* = 1.6 Hz, 1H), 2.74 (t, *J* = 7.5 Hz, 2H), 1.76 (tt, *J* = 7,5, 7.5 Hz, 2H), 1.28-1.36 (br, 6H), 0.90 (t, *J* = 7.5 Hz, 3H). ^{13}C-NMR (75 MHz, CD$_2$Cl$_2$, δ): 139.95, 138.69, 134.98, 126.62, 121.78, 119.86, 31.59, 29.86, 29.01, 28.61, 26.91, 22.59, 13.82. HRMS (EI) *m/z*: [M]$^+$ calcd for C$_{12}$H$_{16}$S$_2$, 224.0693; found, 224.0694.
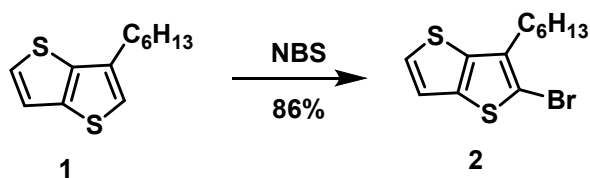
2-Bromo-3-hexylthieno[3,2-*b*]thiophene (2). Compound 1 (3.00 g, 13.4 mmol) was dissolved in a solution of chloroform. Then *N*-bromosuccinimide (2.49 g, 14.0 mmol) was added in portions at 0°C. After the mixture was stirred for 2 h at room temperature, water was added to quench the reaction. The aqueous layer was extracted with dichloromethane, and the organic layer was washed with brine. After the mixture was dried over anhydrous Na$_2$SO$_4$, the organic solvent was removed under vacuum. The residue was purified by chromatography on silica gel eluting with petroleum ether to give the title compound (3.49 g, 86%). ^{1}H NMR (300 MHz, CD$_2$Cl$_2$, δ): 7.43 (d, *J* = 5.2 Hz, 1H), 7,20 (d, *J* = 5.2 Hz, 1H), 2.76 (t, *J* = 7.5 Hz, 2H), 1.72 (tt, *J* = 7.5, 7.5 Hz, 2H), 1.29-1.40 (br, 6H), 0.90 (t, *J* = 7.5 Hz, 3H). ^{13}C NMR (75 MHz, CD$_2$Cl$_2$, δ): 138.39, 136.88, 134.27, 125.98, 119.44, 109.97, 31.57, 29.13, 28.95, 28.01, 22.59, 13.85. MS (EI) *m/z*: [M]$^+$ calcd for C$_{12}$H$_{15}$BrS$_2$, 301.98 (^{79}Br), 303.98 (^{81}Br); found, 301.98 (^{79}Br), 303.98 (^{81}Br).
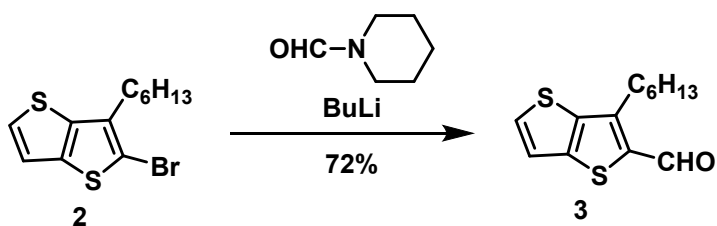
3-Hexylthieno[3,2-*b*]thiophene-2-carbaldehyde (3). To a 100-mL round-bottomed flask under a N_2 atmosphere, compound 2 (5.00 g, 16.5 mmol) and 40 mL of dry THF was added. Then n-butyl lithium (6.93 mL, 2.5 M in hexane) was added dropwise to the mixture at −78°C. After the mixture was stirred at −78°C for 0.5 h, 1-formylpiperidine (2.82 g, 29.0 mmol) was added. Then the mixture was stirred overnight at room temperature. Water was added to quench the reaction, and the product was extracted with ethyl acetate. After the mixture was dried with anhydrous Na_2SO_4, 3 (3.01 g, 72.3%) was purified by silica gel chromatography with 15% ethyl acetate/hexane as eluent to afford a yellow oil. ^{1}H NMR (300 MHz, CD_2Cl_2, δ): 10.09 (s, 1H), 7.63 (d, J = 5.3 Hz, 1H), 7,27 (d, J = 5.3 Hz, 1H), 3.09 (t, J = 7.5 Hz, 2H), 1.79 (tt, J = 7.5, 7.5 Hz, 2H), 1.31-1.38 (br, 6H), 0.87 (t, J = 7.5 Hz, 3H). ^{13}C NMR (75 MHz, CD_2Cl_2, δ): 182.60, 145.06, 144.32, 141.08, 139.17, 133.01, 120.50, 31.47, 29.95, 29.10, 28.33, 22.52, 14.05. MS (EI) *m/z*: $[M]^+$ calcd for $C_{13}H_{16}OS_2$, 252.06; found, 252.07.
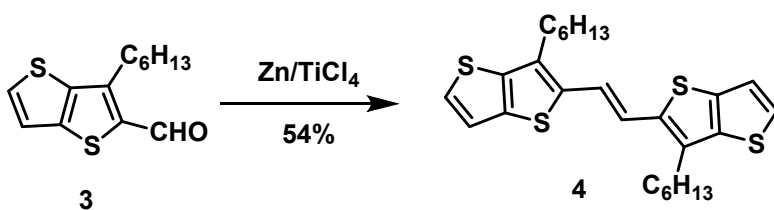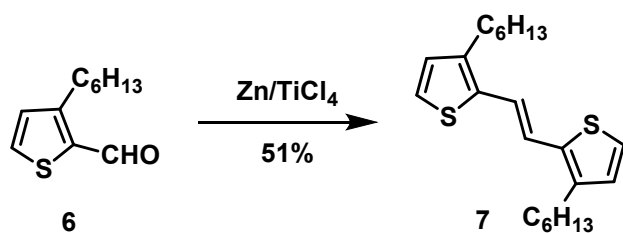

(*E*)-1,2-Bis(3-hexylthieno[3,2-*b*]thiophen-2-yl)ethene (4). To a stirred suspension of zinc powder (2.35 g, 36.0 mmol) in anhydrous tetrahydrofuran (50 mL) under a N_2 atmosphere, $TiCl_4$ (19.0 mL, 1 M in toluene) was added using a syringe at 0°C. Then the mixture was heated at 70 °C for 6 h and the suspension was allowed to cool to room temperature. 3 (2.27 g, 9 mmol) was added, and the solution was then refluxed overnight. After the reaction was completed, saturated sodium carbonate solution was added to the mixture. Then the mixture

6

was passed through a Celite pad, and washed with dichloromethane. The filtrate was washed

with brine and dried with anhydrous Na_2SO_4. Then the title compound was purified by silica

gel chromatography with hexane to afford a bright yellow solid. (1.14 g, 53.6%). ^1H NMR

(300 MHz, CD_2Cl_2, δ): 7.42 (d, J = 5.2 Hz, 2H), 7.26 (d, J = 5.2 Hz, 2H), 7.14 (s, 2H), 2.88 (t,

J = 7.5 Hz, 4H), 1.78 (m, 4H), 1.36-1.47 (m, 12H), 0.96 (t, J = 7.5 Hz, 6H). ^{13}C NMR (75

MHz, CD_2Cl_2, δ): 141.49, 138.36, 135.77, 133.02, 127.07, 119.91, 119.83, 31.61, 29.27,

29.11, 28.18, 22.62, 13.88. HRMS (TOF) m/z: $[M]^+$ calcd for $C_{28}H_{32}S_4$, 472.138136; found,

472.138292.
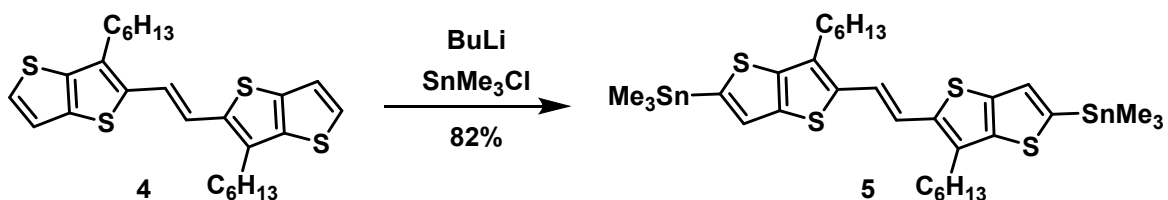
(E)-1,2-Bis(5-(trimethylstannyl)-3-hexylthieno[3,2-b]thiophen-2-yl)ethene (5). 4 (2.00 g, 4.23

mmol) was dissolved in 40 mL of anhydrous THF and the solution was cooled down to

−78°C. Then n-BuLi (3.45 mL, 2.5 M in hexane) was added dropwise to the solution. The

suspension was stirred for 1h at −30 °C, and then cooled down to −78°C. Then a 1.0 M

solution of trimethyltin chloride (9 mL) in hexane was added and then the mixture was stirred

at −30°C for 3 h. Then the mixture was quenched with water, and extracted with

dichloromethane. The combined organic extracts were dried over anhydrous Na_2SO_4 and

concentrated to obtain a crude solid. The target compound was purified by recrystallization

from dichloromethane and methanol to give an orange solid (2.78 g, 82.2 %). ^1H NMR (300

MHz, CD_2Cl_2, δ): 7.05 (s, 2H), 6.89 (s, 2H), 2.63 (t, J = 7.5 Hz, 4H), 1.54 (tt, J = 6, 9 Hz,

4H), 1.12-1.23 (br, 12H), 0.70 (t, J = 6 Hz, 6H), 0.22 (s, 18H). ^{13}C NMR (75 MHz, CD_2Cl_2,

δ): 147.10, 141.63, 138.33, 137.53, 132.53, 126.95, 119.81, 31.62, 29.29, 29.12, 28.29, 22.62,

13.87, −8.53. HRMS (TOF) m/z: $[M]^+$ calcd for $C_{34}H_{48}S_4Sn_2$, 800.068087; found,

800.068011.

3-Hexylthiophene-2-carbaldehyde (6) was synthesized by following the literature methods.[2]

(E)-1,2-Bis(3-hexylthiophen-2-yl)ethene (7): To a stirred suspension of zinc powder (5.00 g, 76.6 mmol) in 100 mL of anhydrous tetrahydrofuran under a N_2 atmosphere, $TiCl_4$ (40.4 mL, 1 M in toluene) was added using a syringe at 0 °C. Then the mixture was stirred at 70°C for 6 h and the suspension was cooled down to room temperature. 6 (3.75 g, 19.1 mmol) was added at once, and the solution was then refluxed overnight. When the reaction was completed, saturated sodium carbonate solution was added to the mixture. Then the mixture was passed through a Celite pad, and washed with hexane. The filtrate was washed with brine and dried with anhydrous Na_2SO_4. Then the title compound was purified by silica gel chromatography with hexane to give a bright yellow solid (3.51 g, 50.9%). ^{1}H NMR (300 MHz, CD_2Cl_2, δ): 7.39 (d, J = 5.2 Hz, 2H), 7.23 (d, J = 5.2 Hz, 2H), 7.10 (s, 2H), 2.84 (t, J = 7.5 Hz, 4H), 1.73 (tt, J = 6, 9 Hz, 4H), 1.31-1.42 (br, 12H), 0.89 (t, J = 7.5 Hz, 6H). ^{13}C NMR (75 MHz, CD_2Cl_2, δ): 140.96, 136.14, 129.87, 122.57, 119.32, 31.67, 30.92, 29.01, 28.34, 22.62, 13.85.
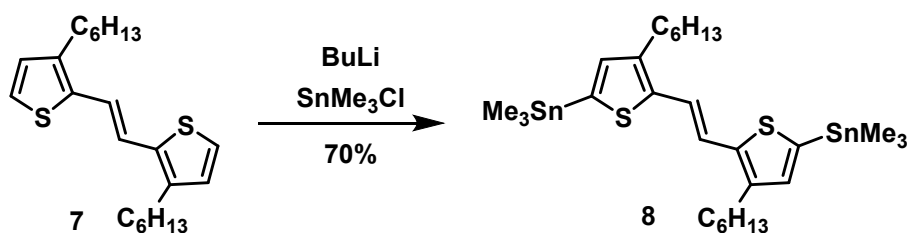
(E)-1,2-Bis(3-hexyl-5-(trimethylstannyl)thiophen-2-yl)ethene: 7 (2 g, 5.55 mmol) was dissolved in 40 mL of anhydrous THF and the solution was cooled down to −78°C. Then n-BuLi (4.66 mL, 2.5 M in hexane) was added dropwise to the solution. The suspension was stirred at −10°C for 1 h, and then cooled down to −78°C. A 1.0 M solution of trimethyltin

chloride (14 mL) in hexane was then added and the mixture was stirred at −30°C for 3 h. Then the mixture was quenched with water, and extracted with dichloromethane. The combined organic extracts were dried over anhydrous Na_2SO_4 and concentrated to crude solid obtained. The target compound was purified by recrystallization from dichloromethane and methanol to give an orange solid (2.67 g, 69.8 %). ^{1}H NMR (300 MHz, CD_2Cl_2, δ): 6.86 (s, 2H), 6.80 (s, 2H), 2.52 (t, J = 7.5 Hz, 4H), 1.45 (tt, J = 7.5, 7.5 Hz, 4H), 1.15-1.25 (br, 12H), 0.76 (t, J = 7.5 Hz, 6H), 0.22 (s, 18H). ^{13}C NMR (75 MHz, CD_2Cl_2, δ): 140.96, 136.14, 129.87, 122.57, 119.32, 31.67, 30.92, 29.01, 28.34, 22.62, 13.85. HRMS (TOF) *m/z*: [M]$^+$ calcd for $C_{28}H_{48}S_4Sn_2$, 688.124278; found, 688.124042.

Synthesis of PT-10-TVT-6, PT-10-DTTE-6, PD-10-TVT-6, PD-10-DTTE-6: In a Schlenk flask, DPP monomers (0.2 mmol), trimethyltin monomers (0.2 mmol), tris(dibenzylideneacetone)dipalladium (0) (4.5 mg) and tri(o-tolyl)phosphine (12.3 mg) were dissolved in dry toluene (5 mL). The flask was charged with nitrogen through a freeze-pump-thaw cycle for three times. Then mixture was stirred at 110°C under nitrogen atmosphere for 24 h. The polymer was precipitated in a mixture of methanol: 1 M aqueous HCl solution (10: 1) after the mixture was cooled to room temperature. The crude polymer was collected by filtration and then purified by Soxhlet extraction with methanol, acetone, hexane, chloroform, and chlorobenzene. Evaporation of the chlorobenzene fraction afforded a dark solid.

PD-10-TVT-6: GPC: M_n = 64.4 kDa, PDI = 2.20; ^{1}H NMR (300 MHz, $C_2D_2Cl_4$, 373 K, δ): 9.1–8.7(br, 4H), 7.4–7.0 (br, 4H), 4.04 (br, 4H), 2.82 (br, 4H), 2.01 (br, 2H), 1.41−1.27 (m, 96H), 0.89 (m, 18H).

PBD-10-TVT-6: GPC: M_n = 49.0 kDa, PDI = 2.15; ^{1}H NMR (300 MHz, $C_2D_2Cl_4$, 373 K, δ): 9.03 (br, 4H), 7.09 (br, 2H), 6.75 (br, 2H), 4.02 (br, 4H), 2.85 (br, 4H), 1.41−0.89 (m, 116H).

PD-10-DTTE-6: GPC: M_n = 48.6 kDa, PDI = 2.52; ^{1}H NMR (300 MHz, C$_2$D$_2$Cl$_4$, 373 K, δ): 9.05 (br, 4H), 7.07 (br, 2H), 6.73 (br, 2H), 4.03 (br, 4H), 2.82 (br, 4H), 1.41–0.89 (m, 116H).

PBD-10-DTTE-6: GPC: M_n = 46.4 kDa, PDI = 2.84; ^{1}H NMR (300 MHz, C$_2$D$_2$Cl$_4$, 373 K, δ): 9.04–8.84 (br, 4H), 7.01 (br, 4H), 4.01 (br, 4H), 2.85 (br, 4H), 1.41–0.89 (m, 116H).

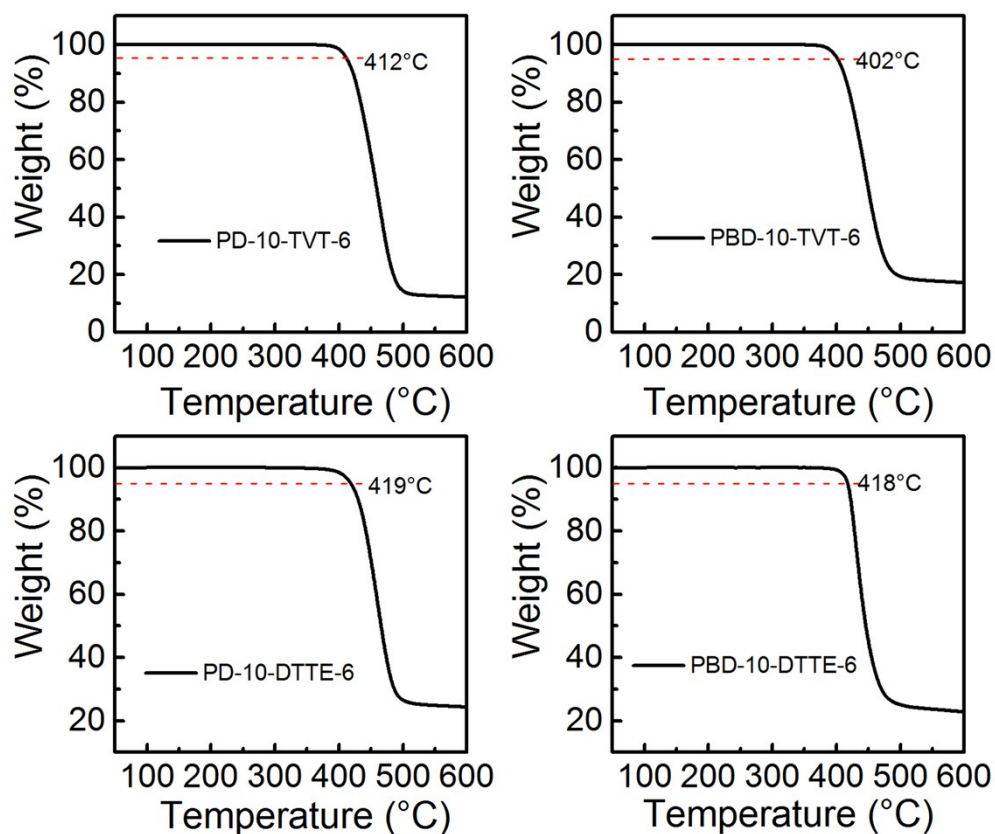2. Thermal, optical and electrochemical properties
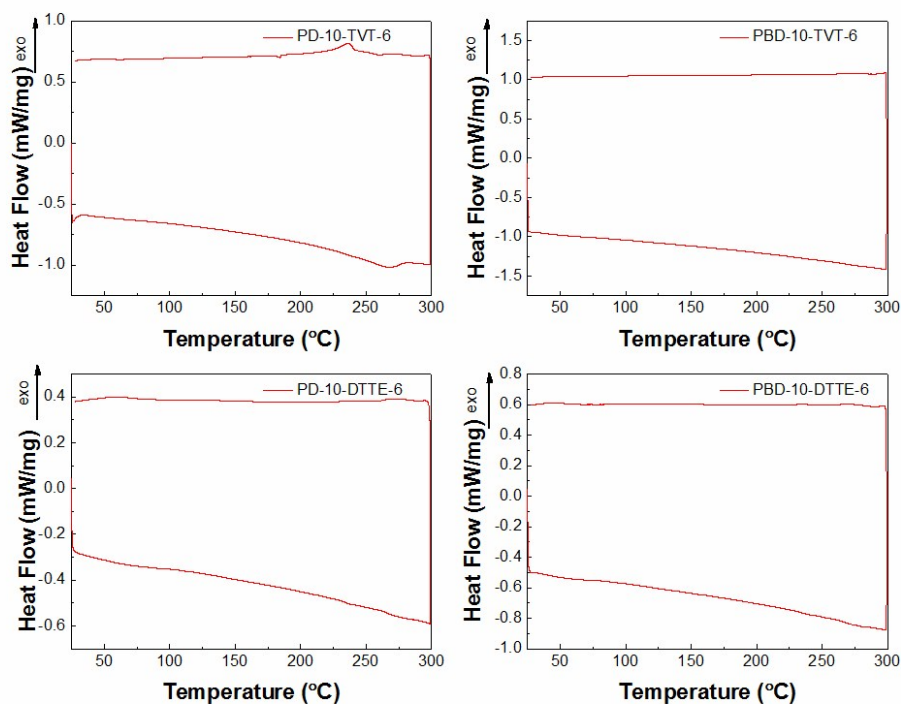

Fig. S1 TGA traces of four polymers.

Fig. S2 DSC traces of four polymers.

Table S1 Optical and electrochemical properties of four polymers.

Polymer	λ_{abs} (nm)		E_g^{opt} (eV)	E_{LUMO} (eV)[a]	E_{HOMO} (eV) [a]	IP (eV)
	soln.	film				
PD-10-TVT-6	818	786	1.32	−3.40	−5.20	4.88
PBD-10-TVT-6	764, 826	752, 816	1.35	−3.39	−5.17	4.84
PD-10-DTTE-6	722, 787	722, 792	1.32	−3.42	−5.20	4.96
PBD-10-DTTE-6	730, 806	722, 800	1.40	−3.40	−5.04	4.86

[a]The values are calculated using the equation $E = [E_{onset(Fc/Fc+ \text{ vs } Ag/AgCl)} − E_{onset} − 4.80]$ eV, where 4.80 eV is the energy level of ferrocene below the vacuum level and the potential $E_{onset(Fc/Fc+ \text{ vs } Ag/AgCl)}$ is 0.40 V during the test.
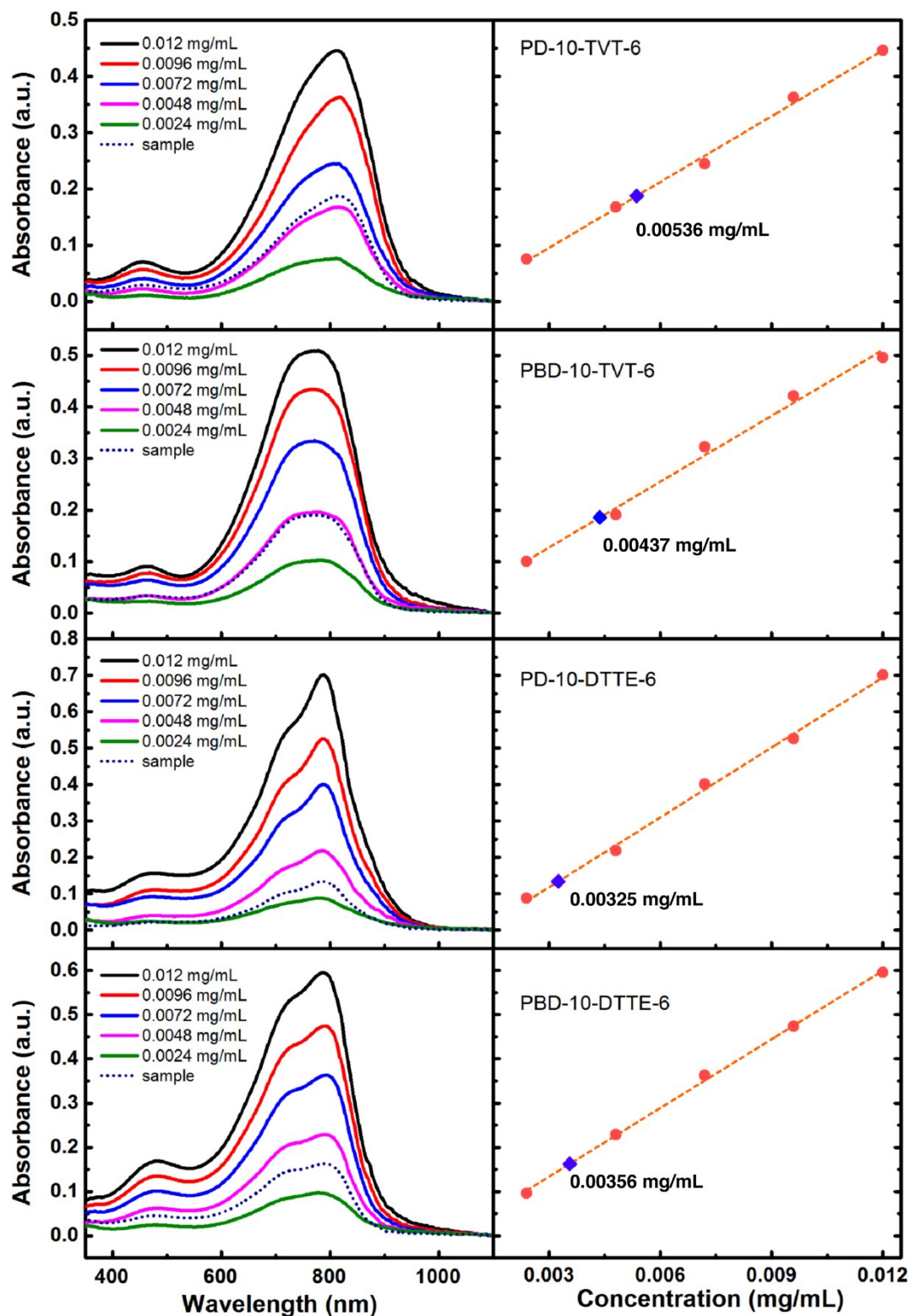
Fig. S3 Absorption spectra of four polymers in o-dichlorobenzene at the concentrations of 0.012, 0.0096, 0.0072, 0.0048, 0.0024 mg mL^{-1} (solid line) and saturated solutions diluted 5000-fold (dot line). Their absorption maxima were fitted using the Beer–Lambert law and the absorption maxima of diluted solutions (blue symbol) were then interpolated to calculate the concentrations.

12
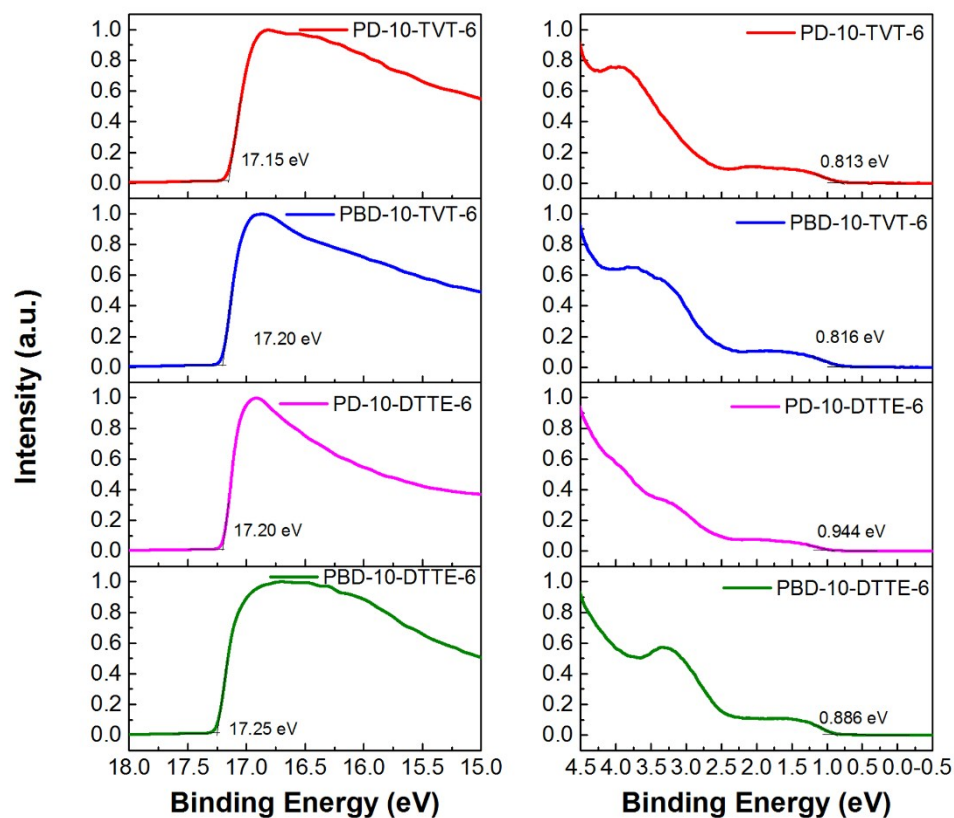
Fig. S4 Ultraviolet photoelectron spectroscopy plots of the four polymers.
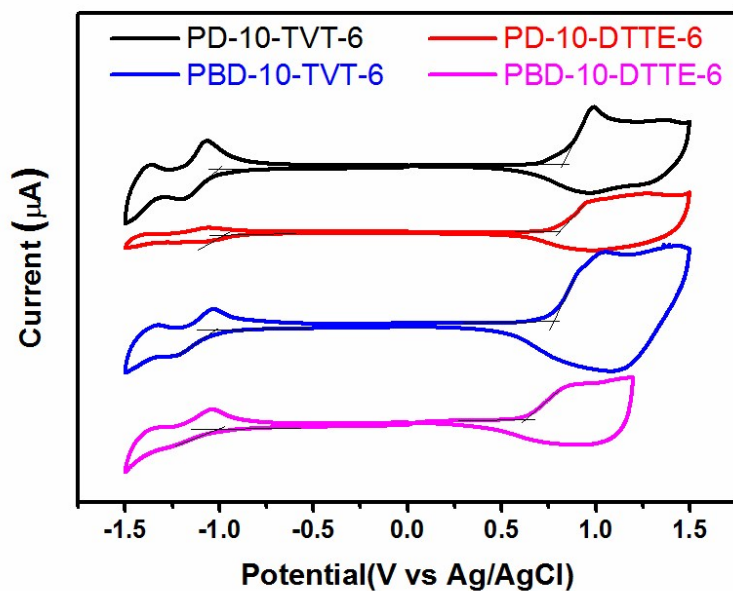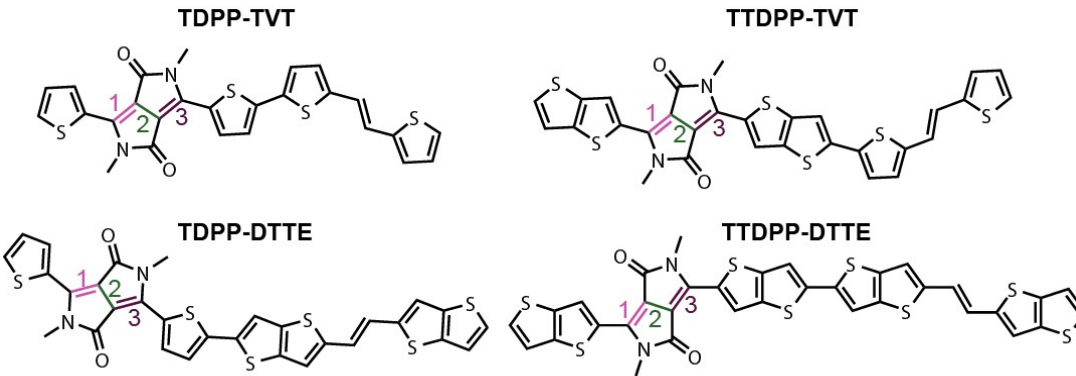
Fig. S5 CV plots of four polymers.

3. Theoretical calculations

The absorption maxima show typical blue shifts with increasing the conjugation length of a co-repeating unit, especially for TT-flanked samples. The PD-10-TVT-6 and PD-10-DTTE-6 thin film both have an optical gap of 1.32 eV whereas those for PBD-10-TVT-6 and PBD-10-DTTE-6 films increase to 1.35 and 1.40 eV, respectively. This phenomenon rationalizes the quinoidal characters of these polymers originating from the intrinsic nature of the low-bandgap diketopyrrolopyrrole moiety.[3] Diketopyrrolopyrrole has a highly polarized bislactam electronic structure with significant single-double bond alternation. Previous reports describe the negative nucleus-independent chemical shift (NICS) value of the DPP ring (−3.3), indicating a weak aromaticity.[4] Moreover, its mesomeric bislactim structure, pyrrolo[3,4-c]pyrrole-1,4-diol, is a fully antiaromatic ring with a NICS(1) value of approximately 3.9. These results suggest the strong quinoidal character of DPP that can be inherited by DPP-based polymers. To illustrate the variation in bond lengths when substituted by different moieties, we calculated the geometry-optimized structure of a co-repeating unit. The bond lengths of DPP moiety in the conjugation pathway are shown in Table S2. Notably, the flanking aromatic moiety, thiophene or thienothiophene, weakens the quinoidal character by equalization of bond lengths, while introduction of TVT or DTTE does not greatly affect the intraring bonds of DPP. Thienothiophene has a more pronounced effect on the bond equalization owing to its extended conjugation, thus leading to a reduced resonance contribution from the low-bandgap quinoidal structure. This theoretical study is consistent with the tendency of optical bandgaps that thienothiophene-flanked PBD-10-TVT-6 and PBD-10-DTTE-6 have wider bandgaps than thiophene-flanked PD-10-TVT-6 and PD-10-DTTE-6.

Table S2 Bond lengths at the respective bond number for DPP-containing monomeric units.

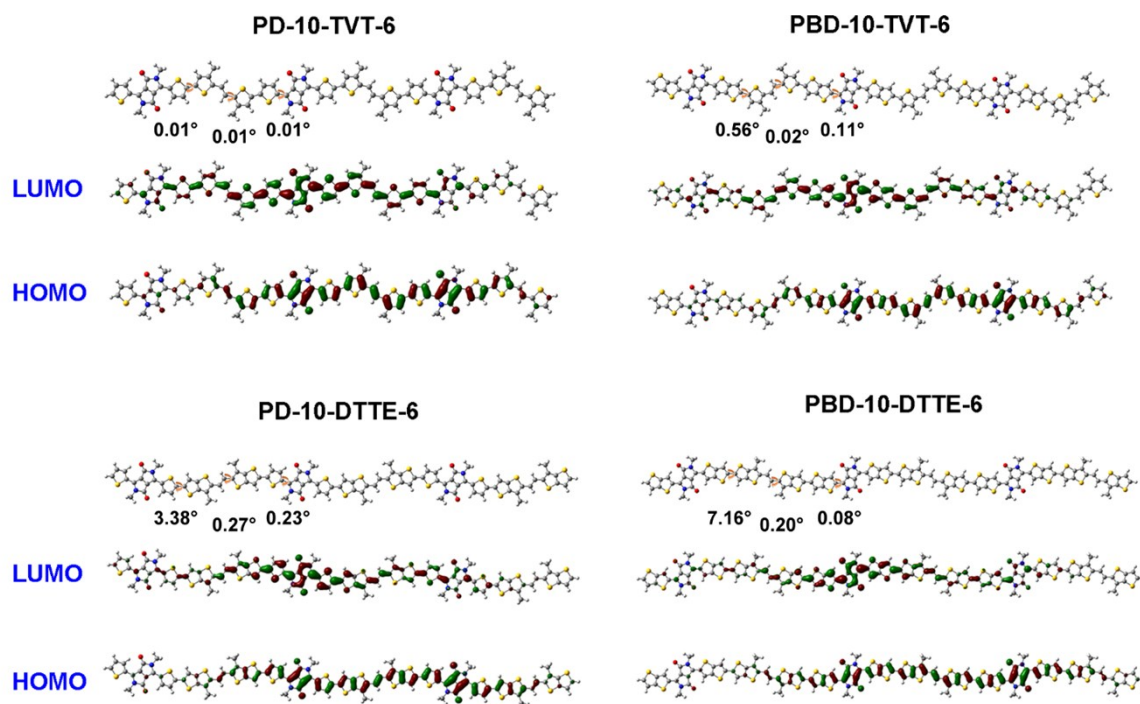| monomeric co-repeating unit	bond length of 1 (Å)	bond length of 2 (Å)	bond length of 3 (Å)
TDPP-TVT	1.3960	1.4203	1.3979
TTDPP-TVT	1.3975	1.4191	1.3986
TDPP-DTTE	1.3961	1.4202	1.3976
TTDPP-DTTE	1.3975	1.4190	1.3985

Fig. S6 Frontier molecular orbital distributions of trimers calculated at the B3LYP/6-31G(d) level of theory.
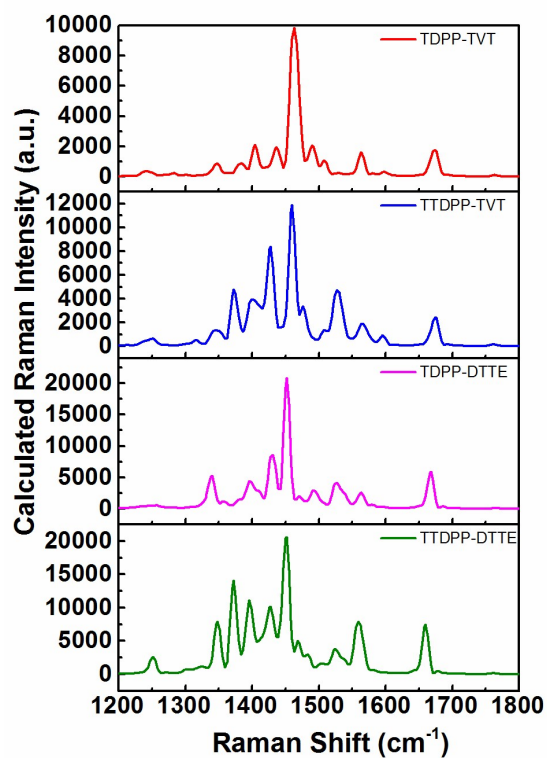
4. Raman spectra

Fig. S7 Calculated Raman spectra of each monomeric co-repeating unit at the B3LYP/6-31G(d) level of theory.
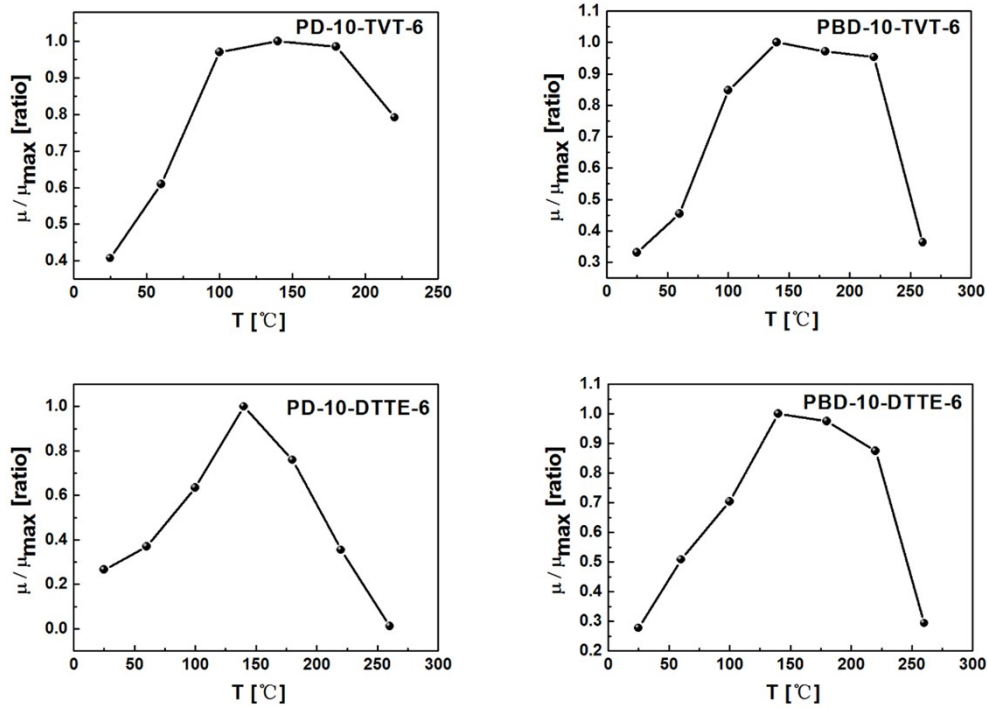
5. Additional information for FET devices

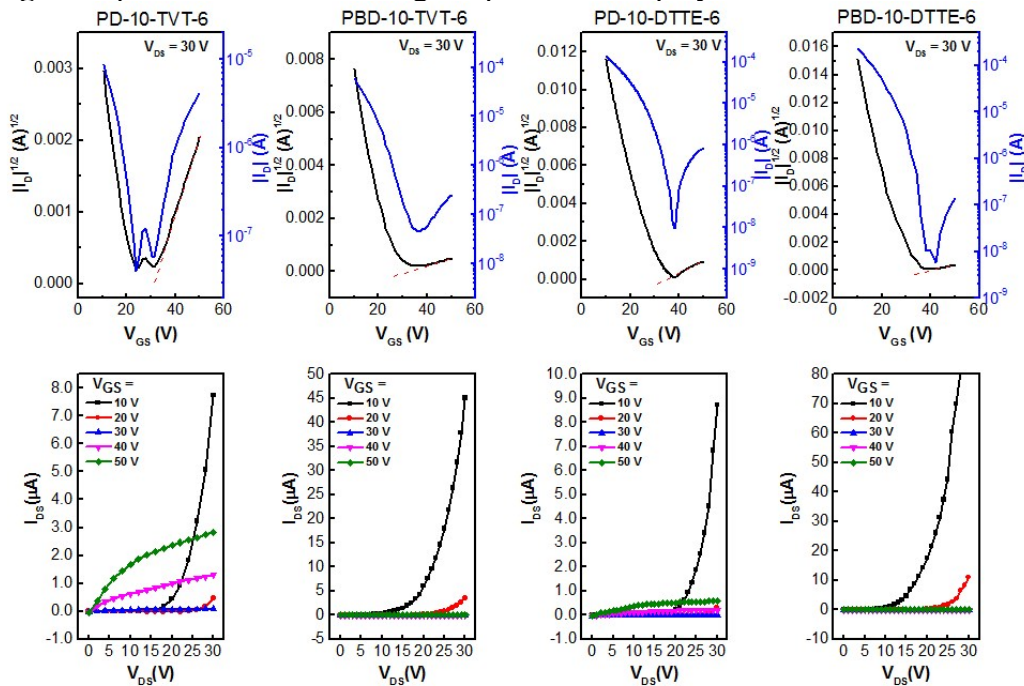**Fig. S8** Optimization of annealing temperatures for polymer-based FETs.

Fig. S9 N-channel transfer and output curves for FETs. The electron mobility was only observed at high gate voltage bias of higher than 40 V, thus low source/drain voltage (30V) was used to preclude the high-field breakdown.
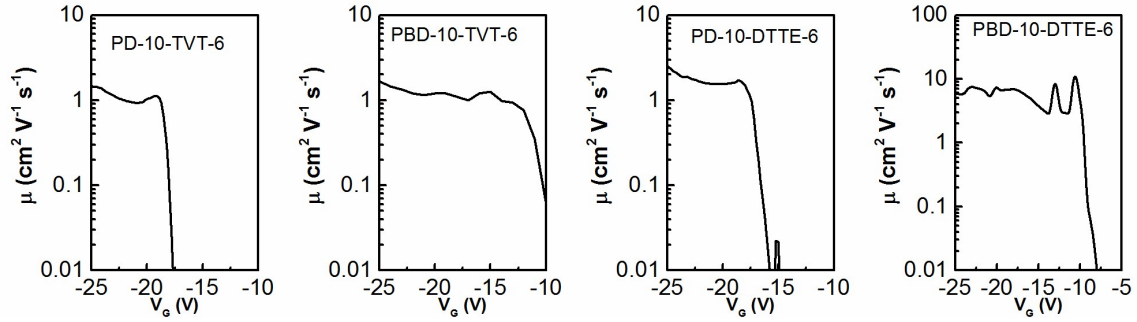
Fig. S10 Gate voltage dependence of mobilities for polymer-based FETs.

The common hysteresis was observed during the devices test, which was normal and acceptable for effective devices measurements according to the recent reports.[5] The slightly decreasing current for backwards scan might be due to the interfacial traps.
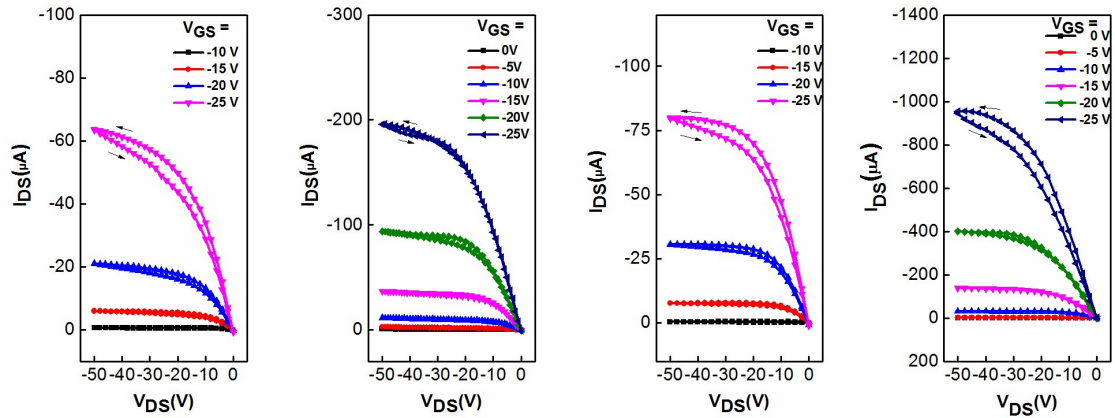
Fig. S11 Forward and reverse sweeps of I-V curves for PD-10-TVT-6, PBD-10-TVT-6 PD-10-DTTE-6, and PBD-10-DTTE-6 polymer-based FETs from left to right, respectively.

To probe into the intrinsic charge transport mechanism, we tested the temperature dependence of the mobility in the range of 120–280 K, as shown in Fig. S12. An Arrhenius-like dependence was observed. Thus, the activation energy was calculated using the Arrhenius equation, $\mu = \mu_0 \exp(-E_a/k_B T)$, where μ is the temperature-dependent mobility, μ_0 the trap-free mobility, E_a the activation energy, and k_B the Boltzmann constant. The extracted activation energies for PD-10-TVT-6, PBD-10-TVT-6, PD-10-DTTE-6, and PBD-10-DTTE-6 are 58.8, 49.8, 46.5, and 42.3 meV, respectively. Such temperature-dependent mobilities are consistent with the multiple-trapping-and-release model. The tendency is in good accordance with the extracted mobilities, suggesting that the extended conjugation length can enhance ordered regions and facilitate intramolecular hopping.
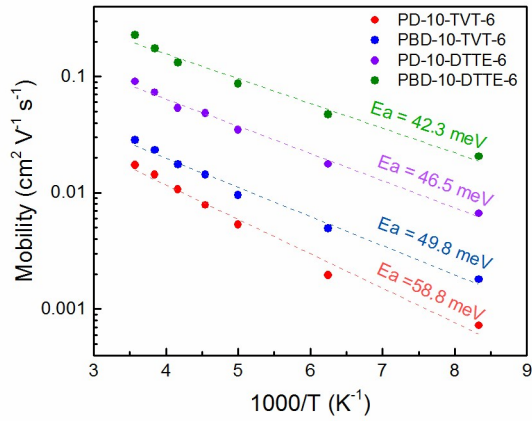
Fig. S12 Temperature-dependent mobilities of four polymers.

Table S3 N-channel Field-Effect Characteristics of Polymer-Based Transistors

polymer	μ_{max} (cm^2 V^{-1} s^{-1})	μ_{ave} (cm^2 V^{-1} s^{-1})	I_{on}/I_{off}	V_{TH} (V)
PD-10-TVT-6	0.0150	0.0133	$> 10^2$	35 ± 6
PBD-10-TVT-6	3.19×10^{-3}	1.46×10^{-3}	$\sim 10^1$	35 ± 5
PD-10-DTTE-6	0.0109	5.00×10^{-3}	$\sim 10^2$	37 ± 4
PBD-10-DTTE-6	2.34×10^{-3}	9.63×10^{-4}	$\sim 10^1$	37 ± 7

6. GIXRD data

Table S4 Microstructure Characterization of Polymer Thin Films

polymer	mode	d-spacing (Å)		coherence length (Å)	
		(100)	(010)	(100)	(010)
PD-10-TVT-6	Out-of-plane	21.7 (21.2)	3.62 (3.62)	38.9 (37.6)	22.6 (20.7)
	In-plane	22.4 (21.8)			
PBD-10-TVT-6	Out-of-plane	21.3 (21.0)	3.62 (3.62)	91.8 (68.1)	
	In-plane		3.61 (3.60)		28.6 (26.1)
PD-10-DTTE-6	Out-of-plane	19.7 (19.2)		84.6 (54.9)	
	In-plane		3.76 (3.76)		22.3 (20.5)
PBD-10-DTTE-6	Out-of-plane	19.6 (19.1)		90.0 (66.1)	
	In-plane		3.54 (3.54)		34.2 (31.2)

[a]The values are related to annealed thin films (140 °C) and the values in parentheses are related to the as-spun ones.
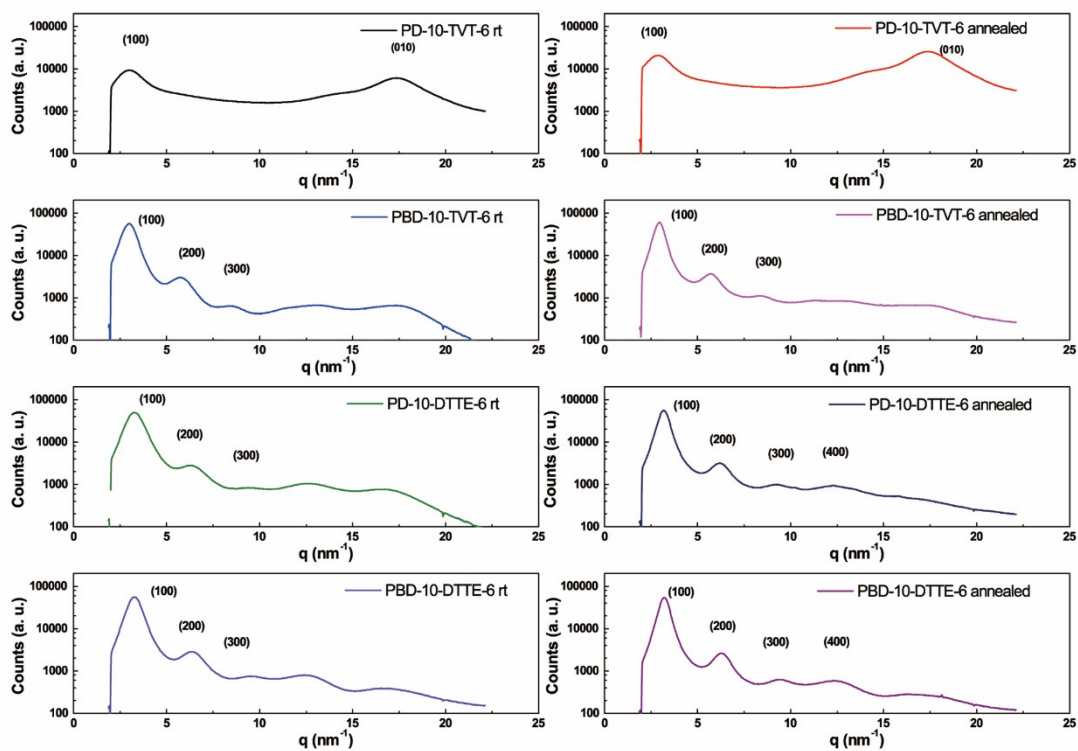
Fig. S13 1D-XRD out-of-plane patterns of four polymer thin films.
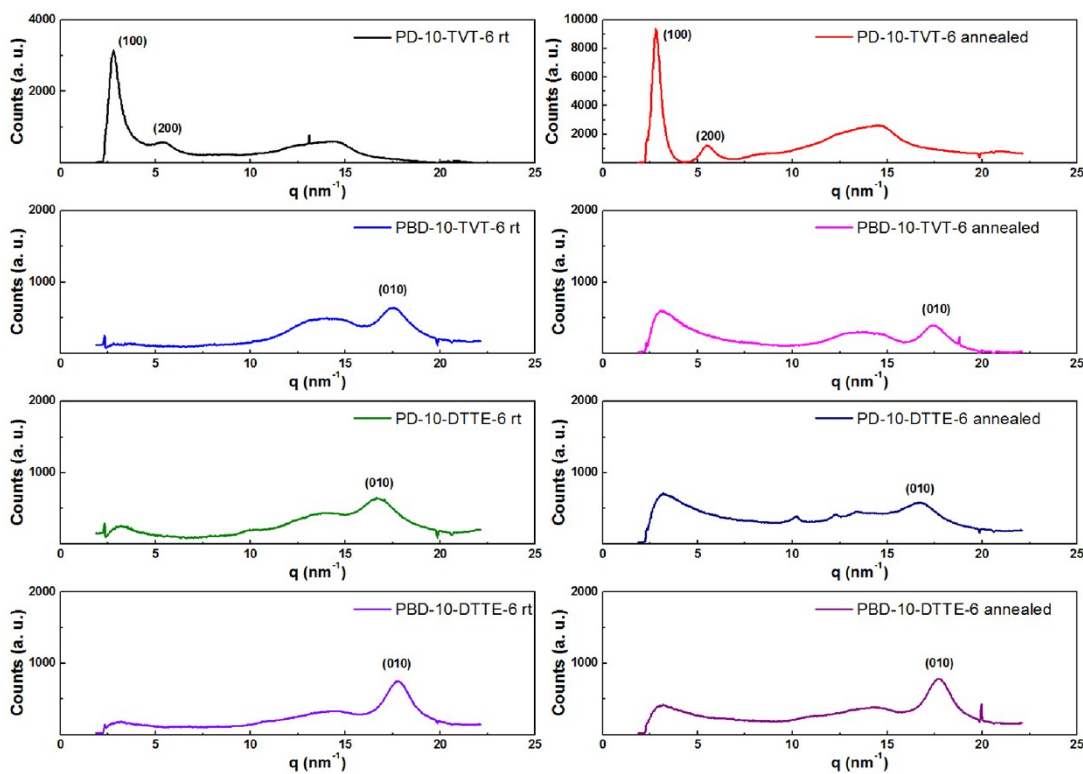
Fig. S14 1D-XRD in-plane patterns of four polymer thin films.
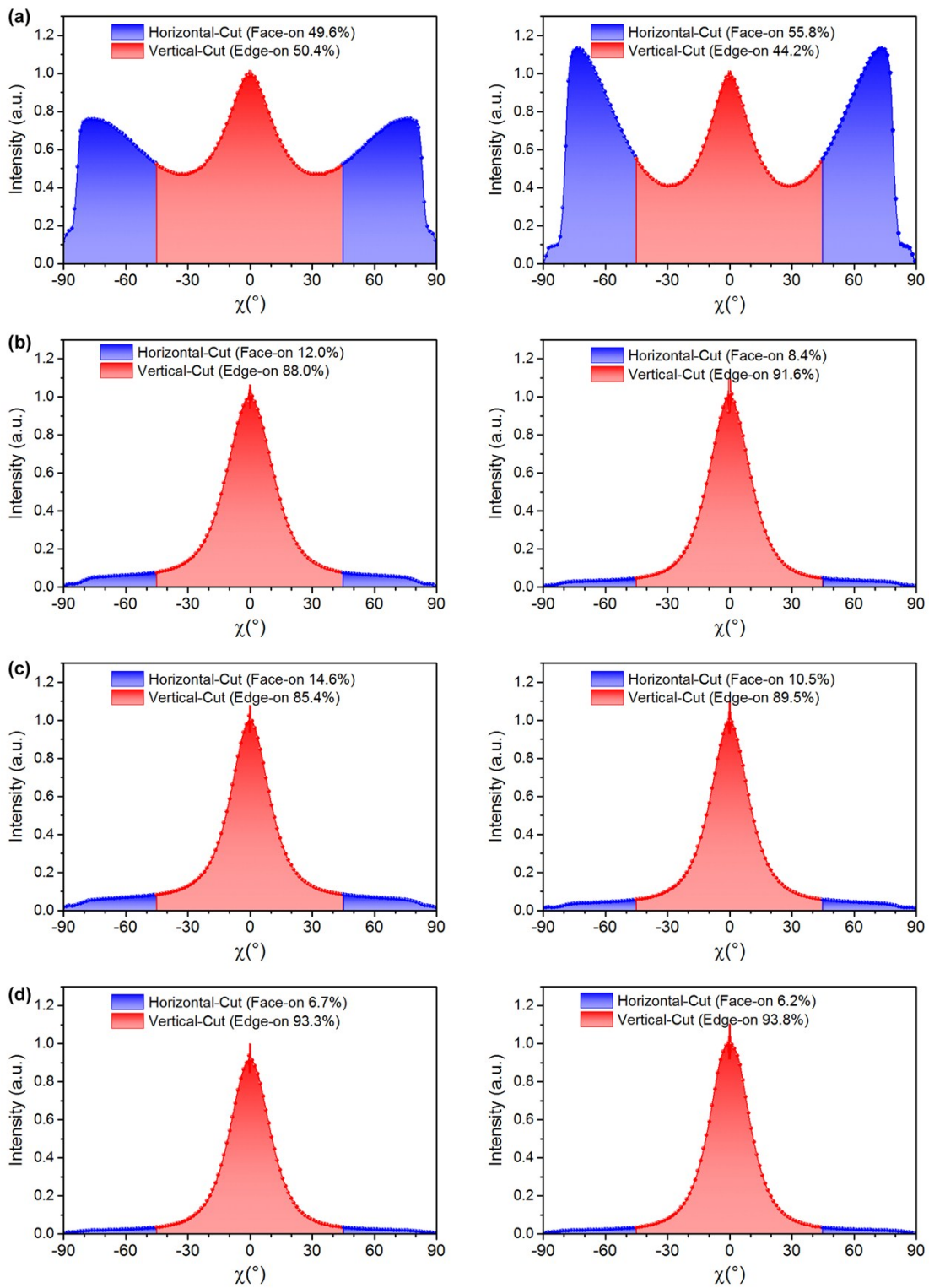
Fig. S15 Pole Fig.s of as-spun (left) and annealed (right) thin films based on (a) PD-10-TVT-6, (b) PBD-10-TVT-6, (c) PD-10-DTTE-6, and (d) PBD-10-DTTE-6.

7. NEXAFS characterization
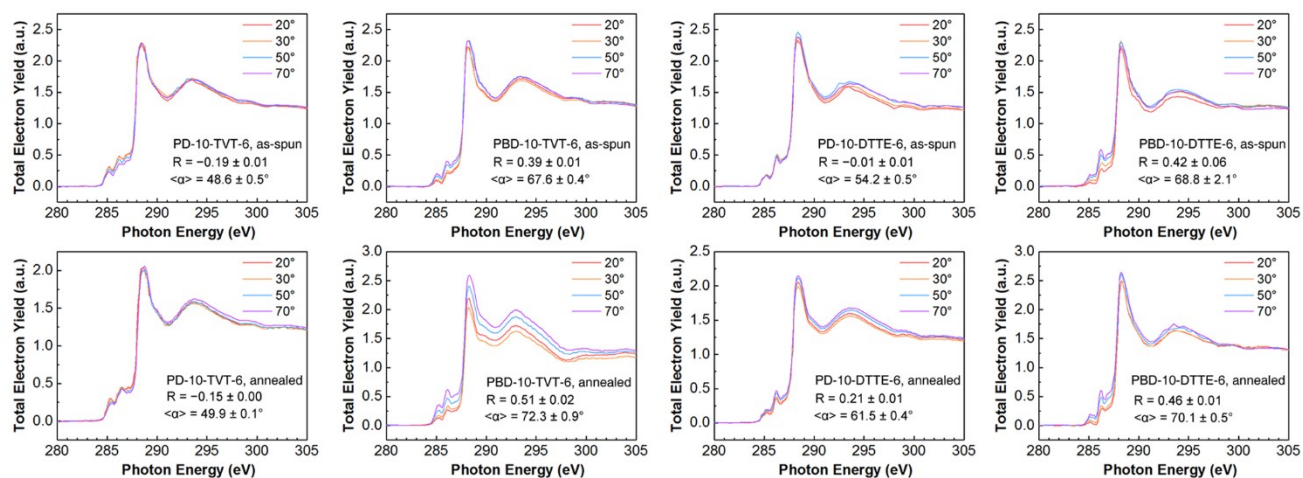
Fig. S16. Angle-resolved NEXAFS spectra of polymer thin films in total electron yield mode. The inset values are the dichroic ratio (R) of the 1s→π* intensity and the average tilt angle (<α>) of polymer backbone.

8. AFM images
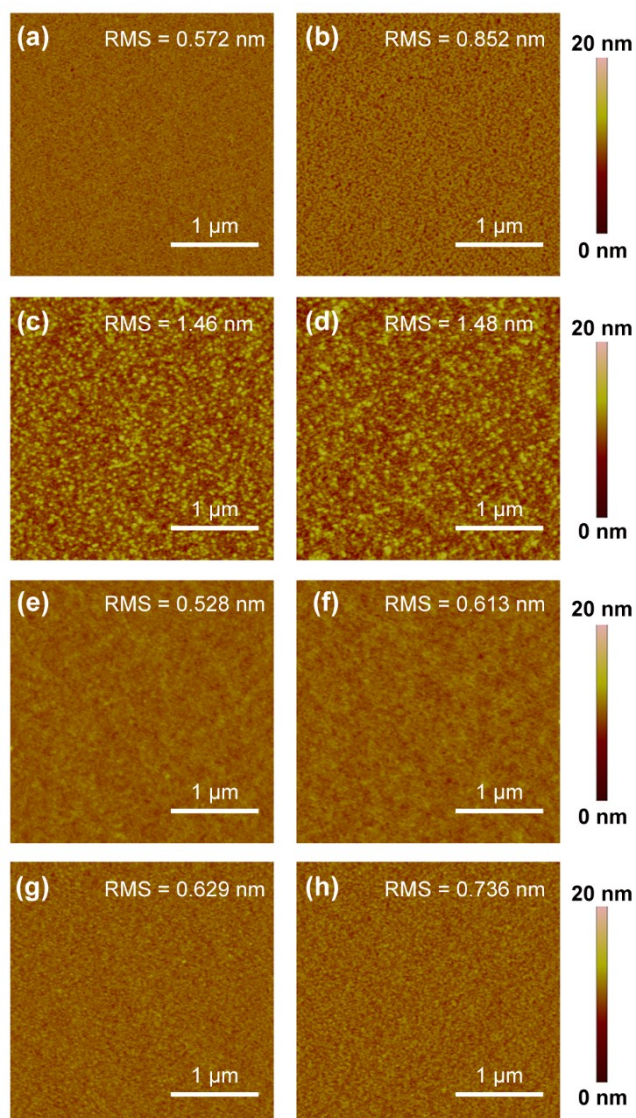
Fig. S17 AFM images of four polymer thin films: (a) as-spun PD-10-TVT-6, (b) annealed PD-10-TVT-6, (c) as-spun PBD-10-TVT-6, (d) annealed PBD-10-TVT-6, (e) as-spun PD-10-DTTE-6, (f) annealed PD-10-DTTE-6, (g) as-spun PBD-10-DTTE-6, and (h) annealed PBD-10-DTTE-6.

9. Schematic view of self-assembly
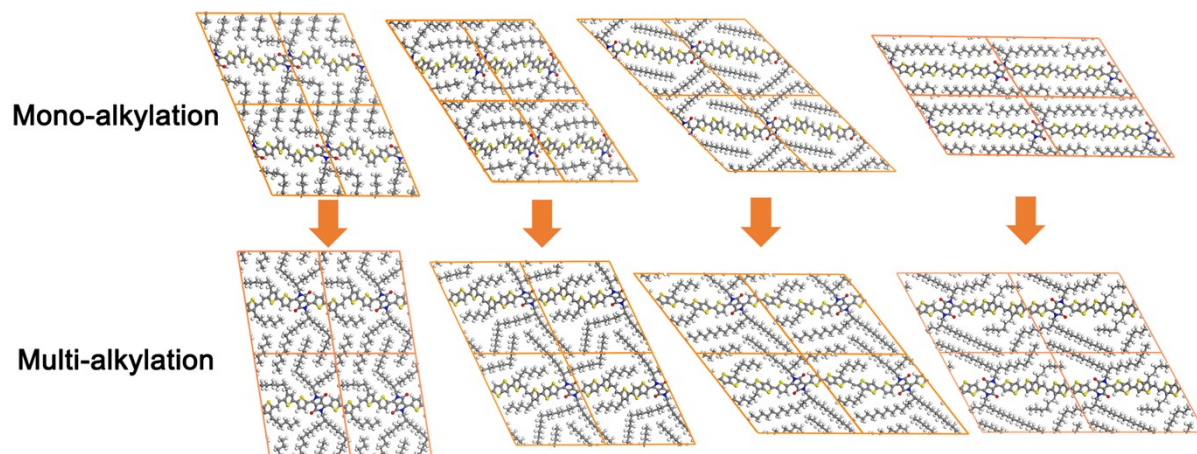
Fig. S18 Schematic view of packing patterns of mono- and multi-alkylated polymers.

10. NMR spectra of new compounds
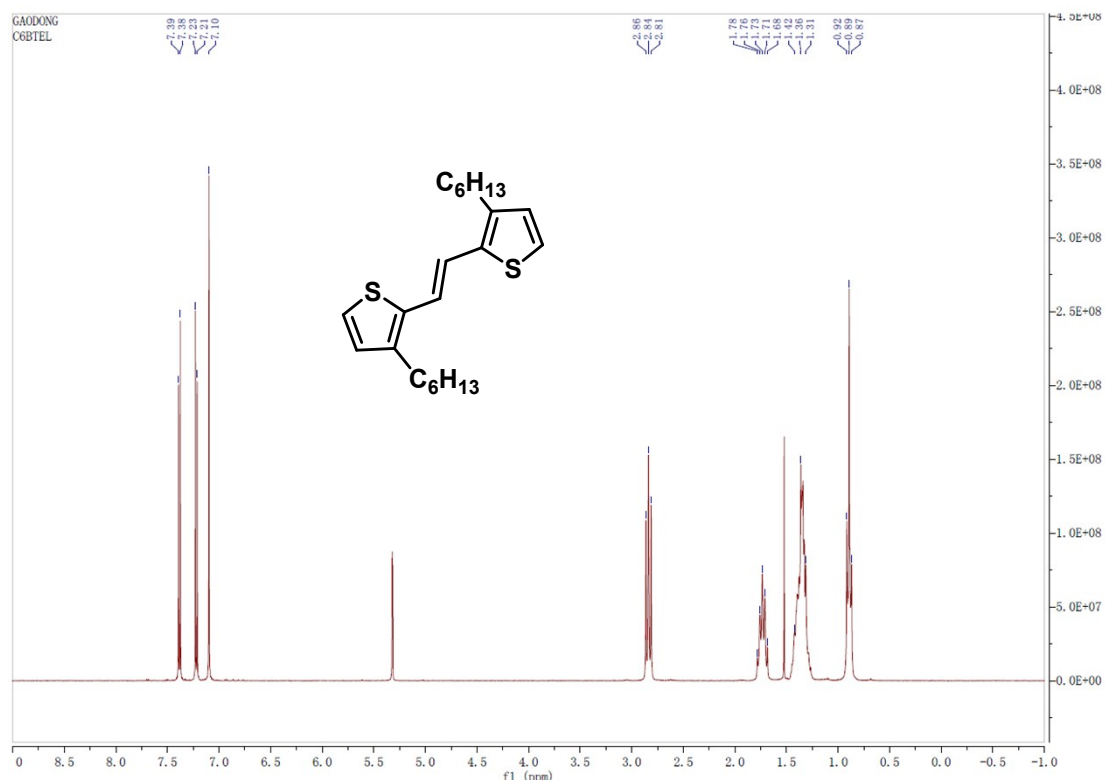
Fig. S19 ^{1}H NMR of (*E*)-1,2-bis(3-hexylthiophen-2-yl)ethene
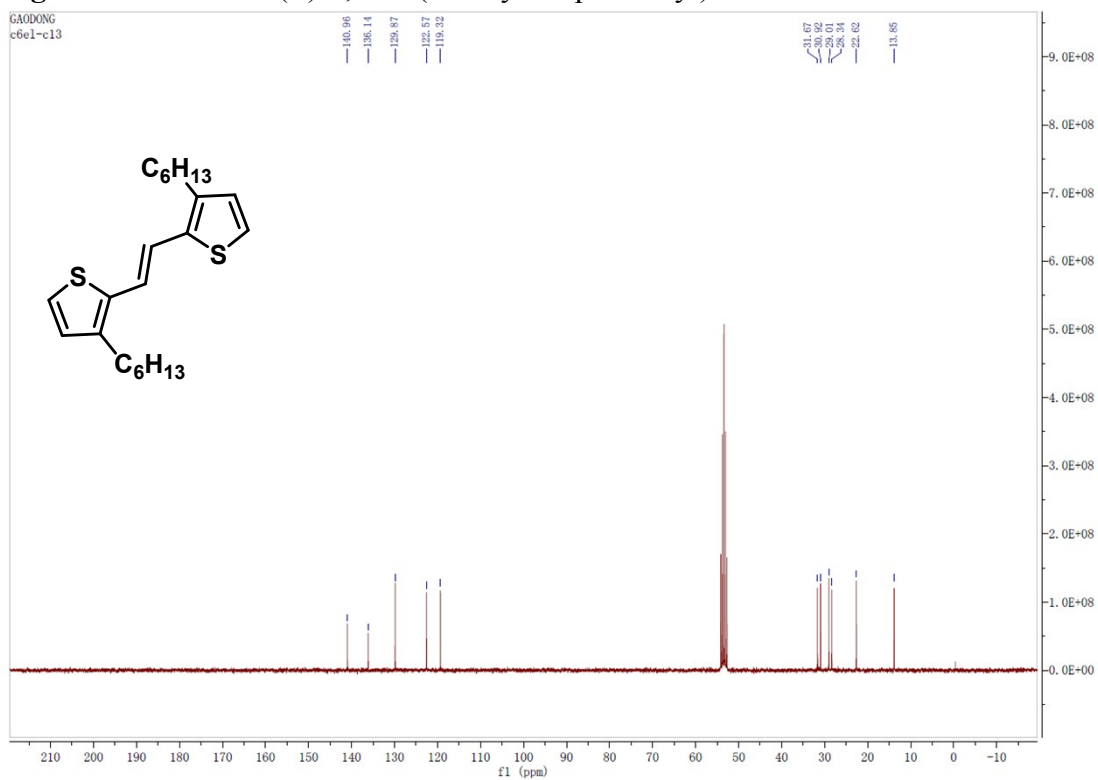
Fig. S20 ^{13}C NMR of (*E*)-1,2-bis(3-hexylthiophen-2-yl)ethene

24
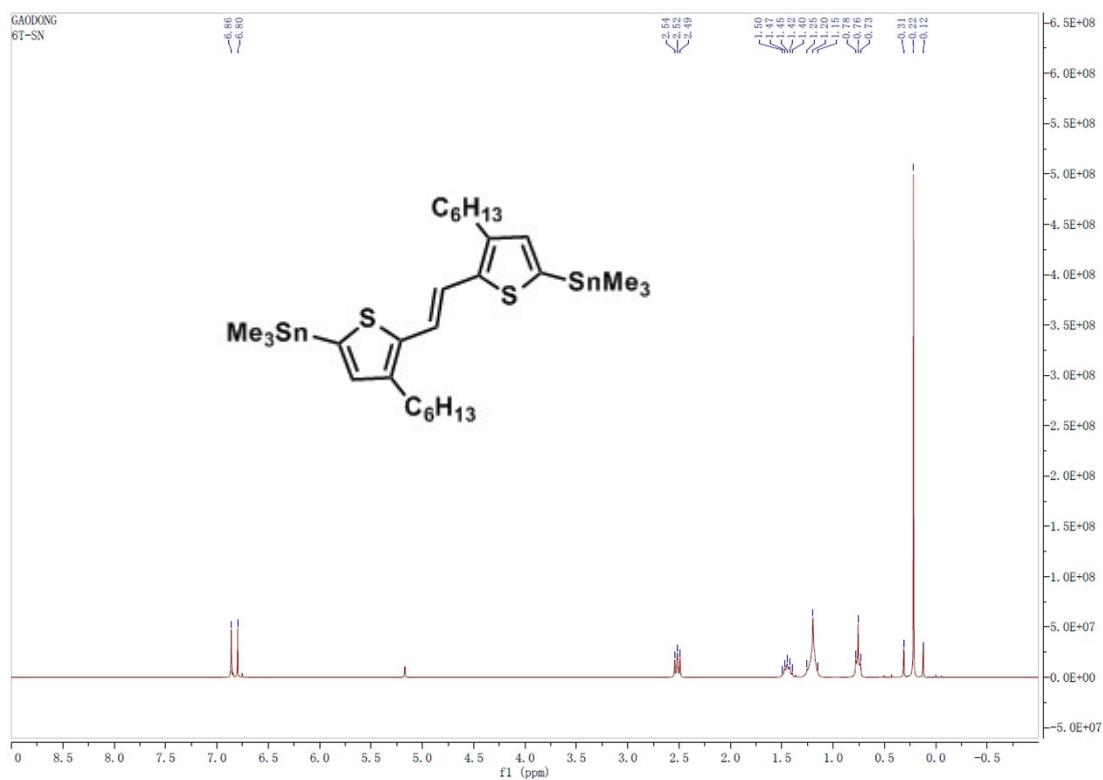
Fig. S21 ^{1}H NMR of (*E*)-1,2-bis(3-hexyl-5-(trimethylstannyl)thiophen-2-yl)ethene
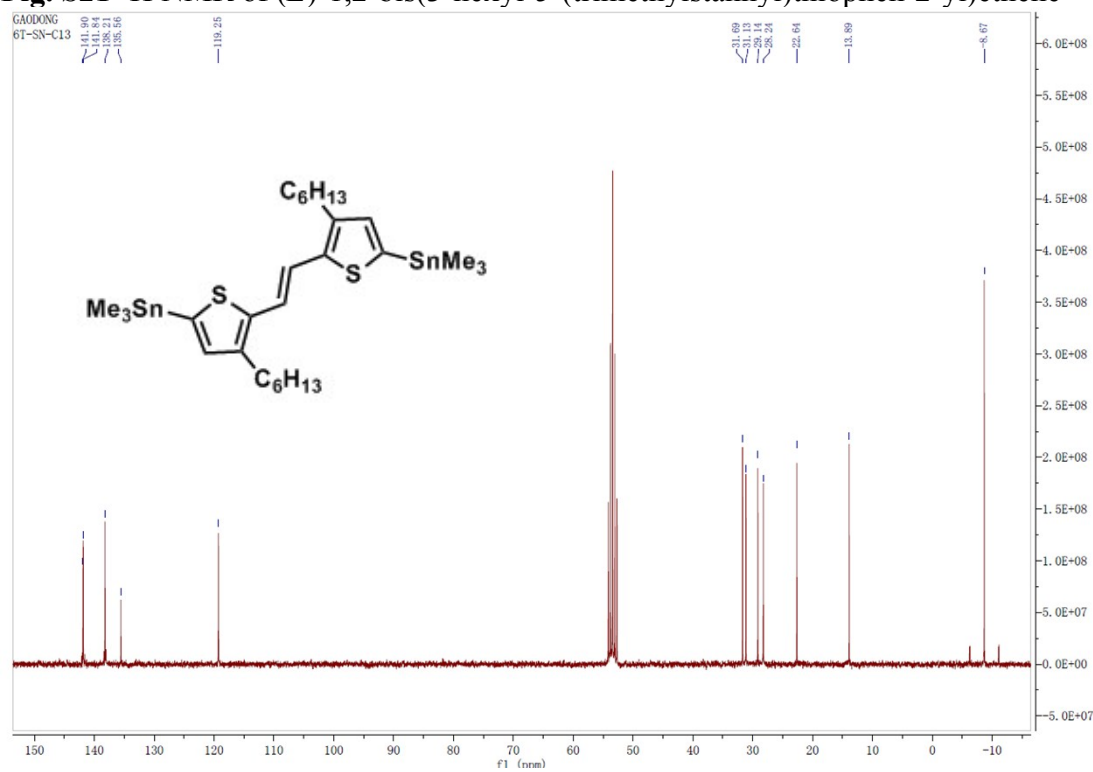
Fig. S22 ^{13}C NMR of (*E*)-1,2-bis(3-hexyl-5-(trimethylstannyl)thiophen-2-yl)ethene
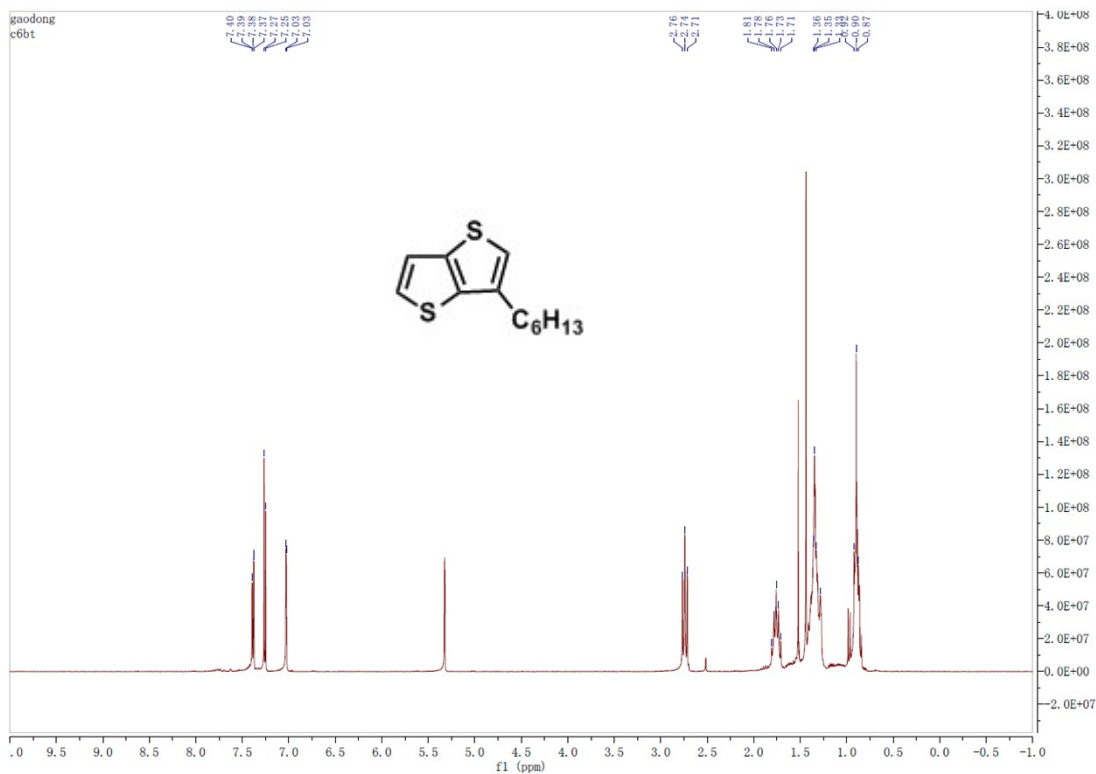
Fig. S23 ^{1}H NMR of 3-hexylthieno[3,2-*b*]thiophene
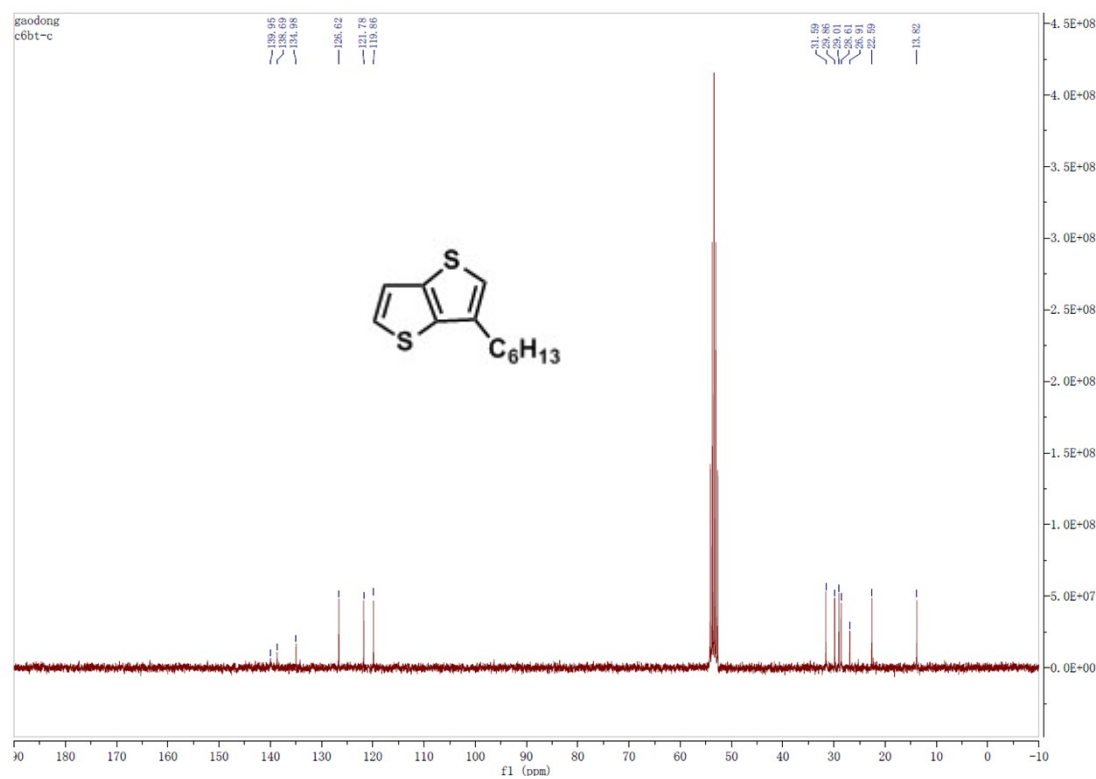
Fig. S24 ^{13}C NMR of 3-hexylthieno[3,2-*b*]thiophene
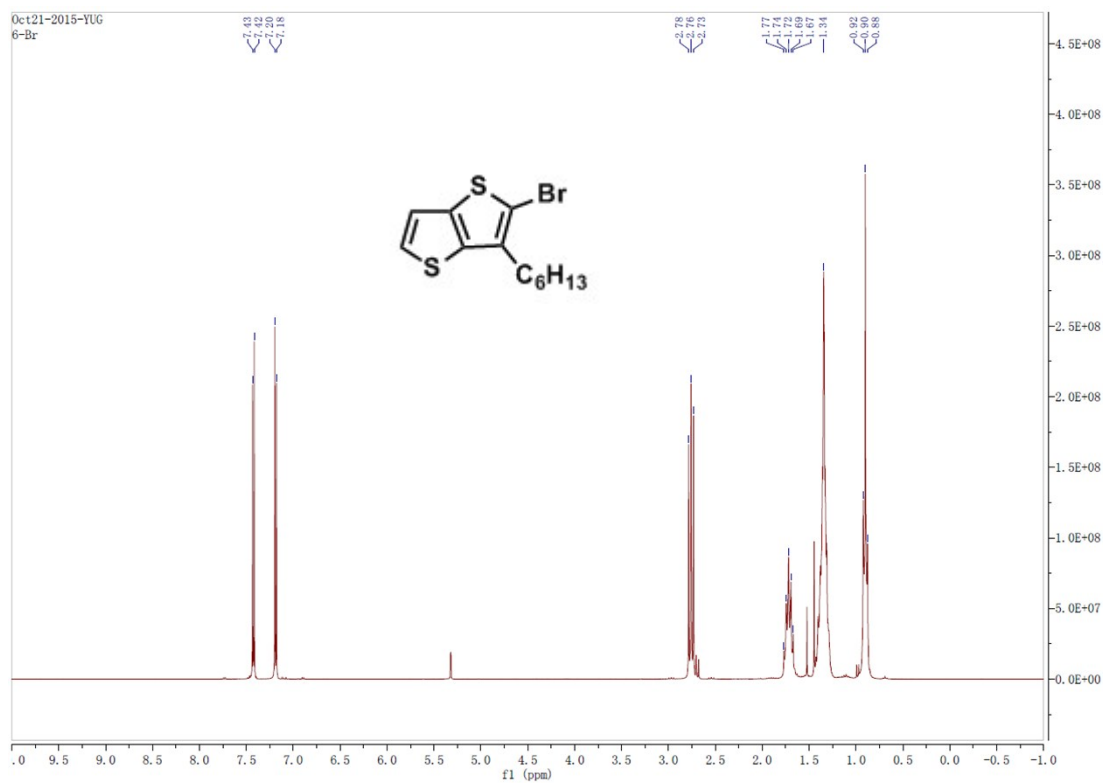
Fig. S25 ^{1}H NMR of 2-bromo-3-hexylthieno[3,2-*b*]thiophene
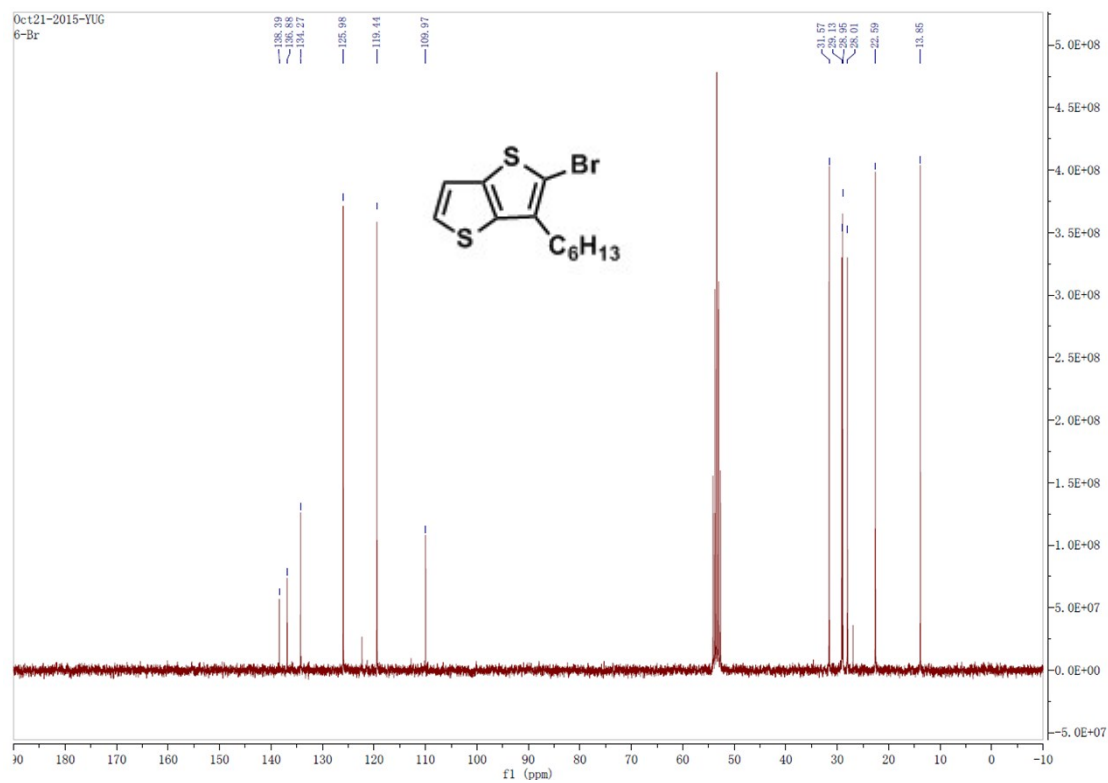
Fig. S26 ^{13}C NMR of 2-bromo-3-hexylthieno[3,2-*b*]thiophene
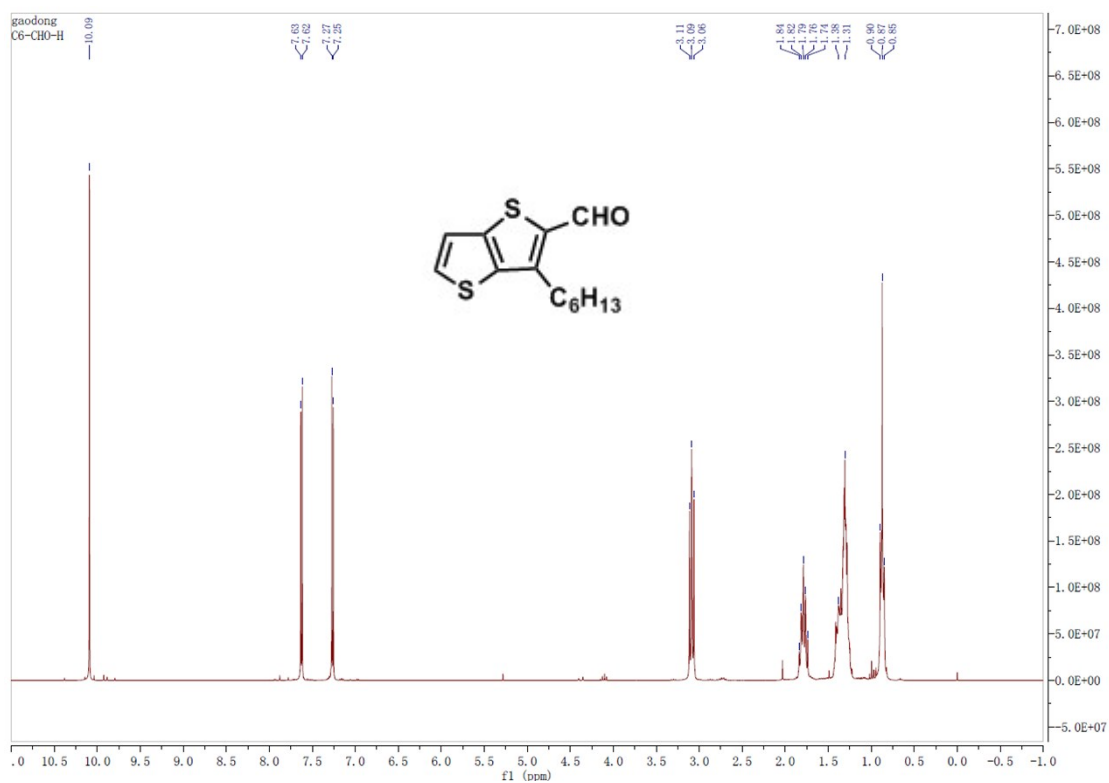
Fig. S27 ¹H NMR of 3-hexylthieno[3,2-*b*]thiophene-2-carbaldehyde
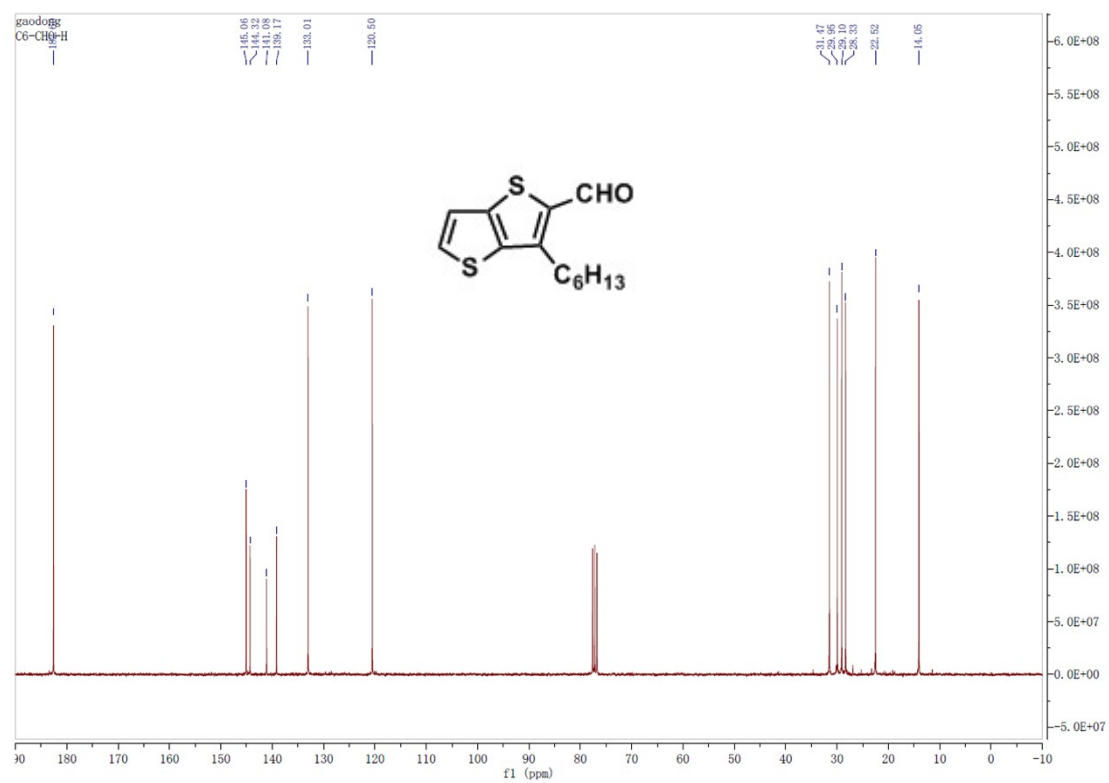
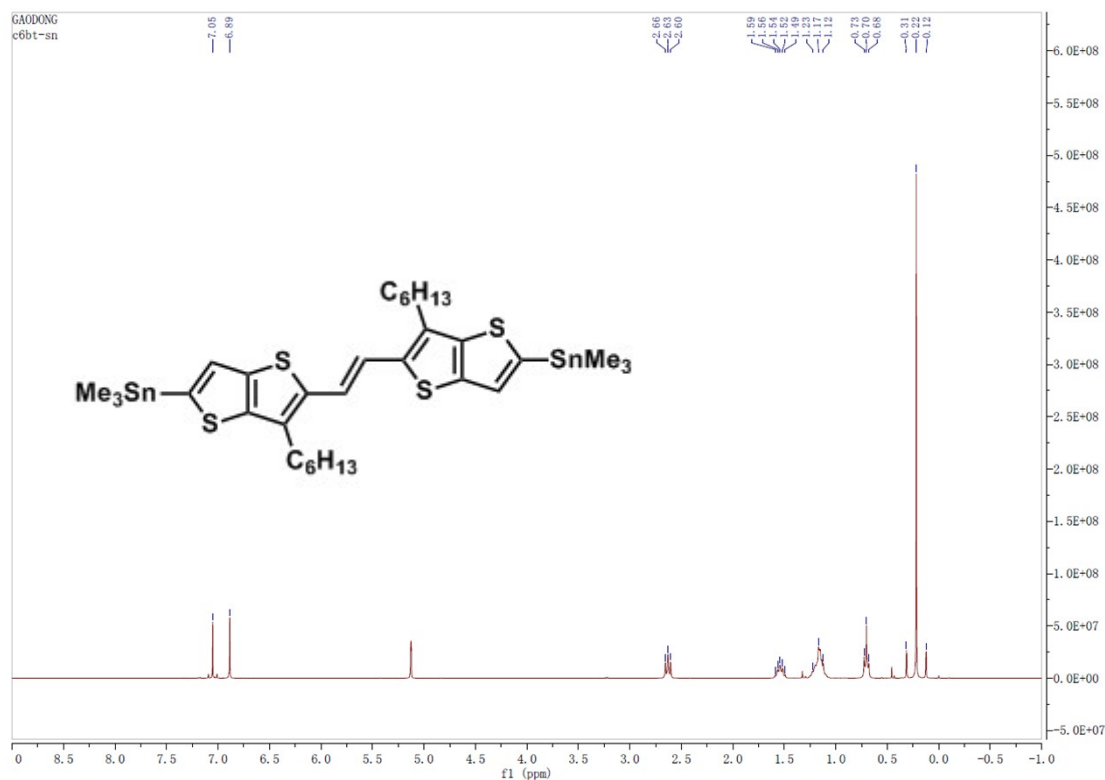**Fig. S28** ¹³C NMR of 3-hexylthieno[3,2-*b*]thiophene-2-carbaldehyde

Fig. S29 ¹H NMR of (*E*)-1,2-bis(3-hexyl-5-(trimethylstannyl)thieno[3,2-*b*]thiophen-2-yl)ethene
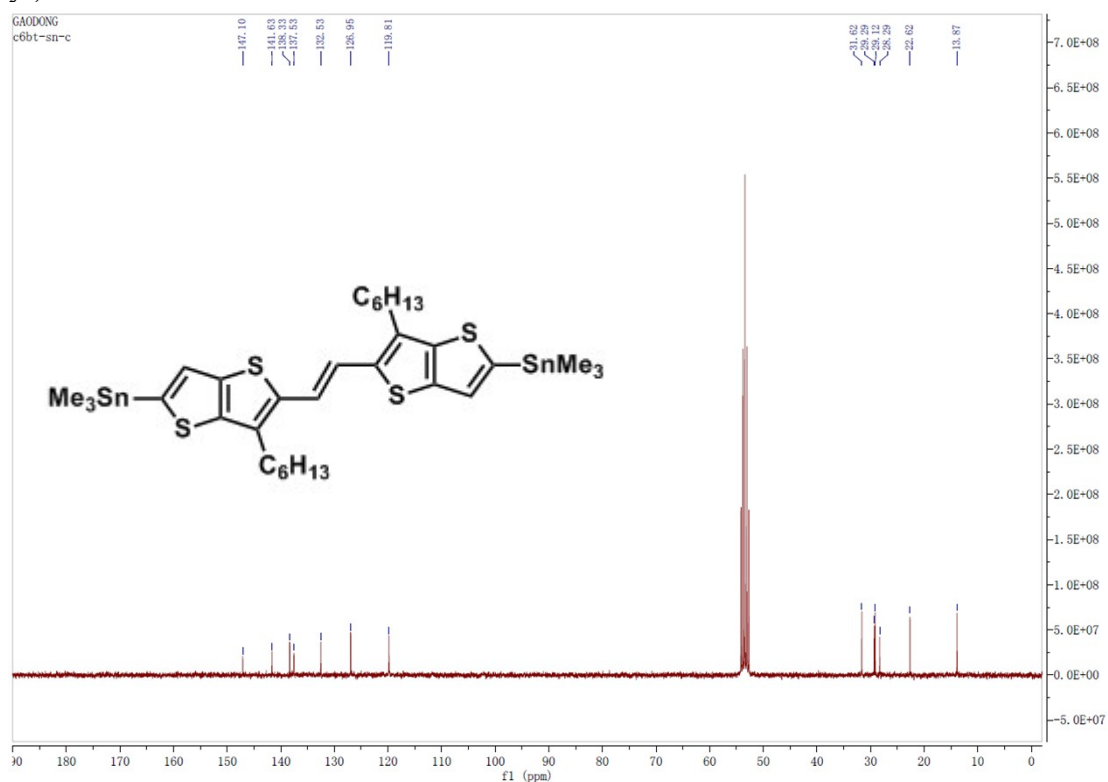

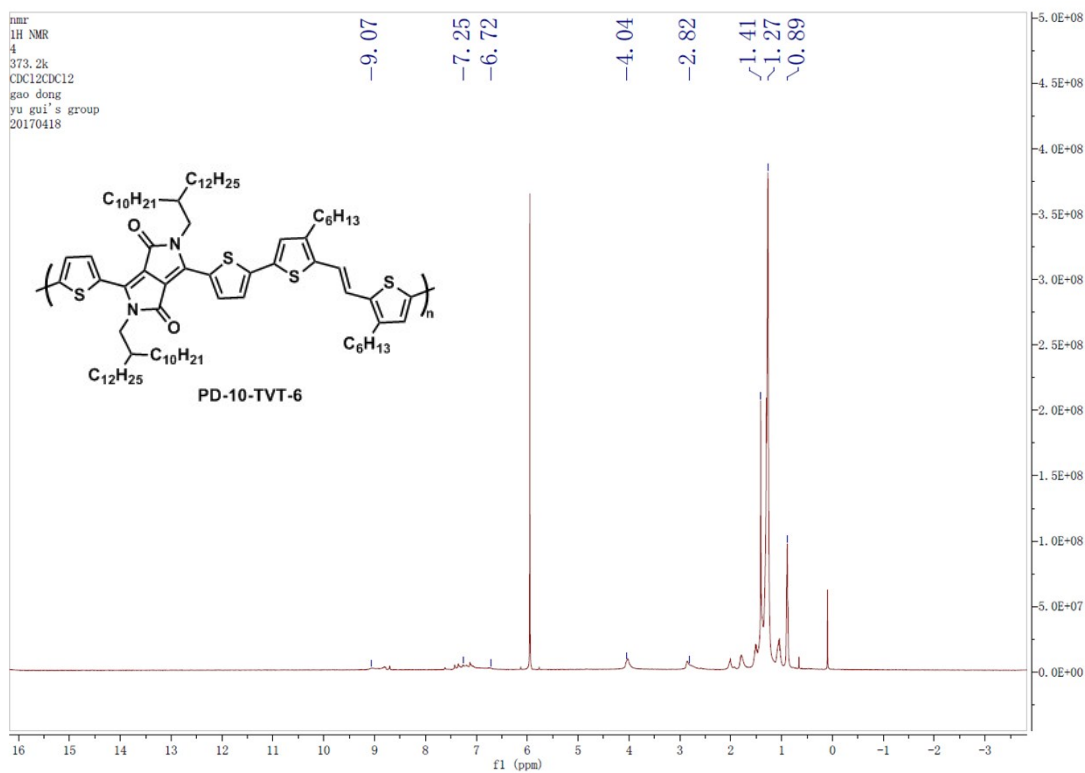**Fig. S30** ¹³C NMR of (*E*)-1,2-bis(3-hexyl-5-(trimethylstannyl)thieno[3,2-*b*]thiophen-2-yl)ethene
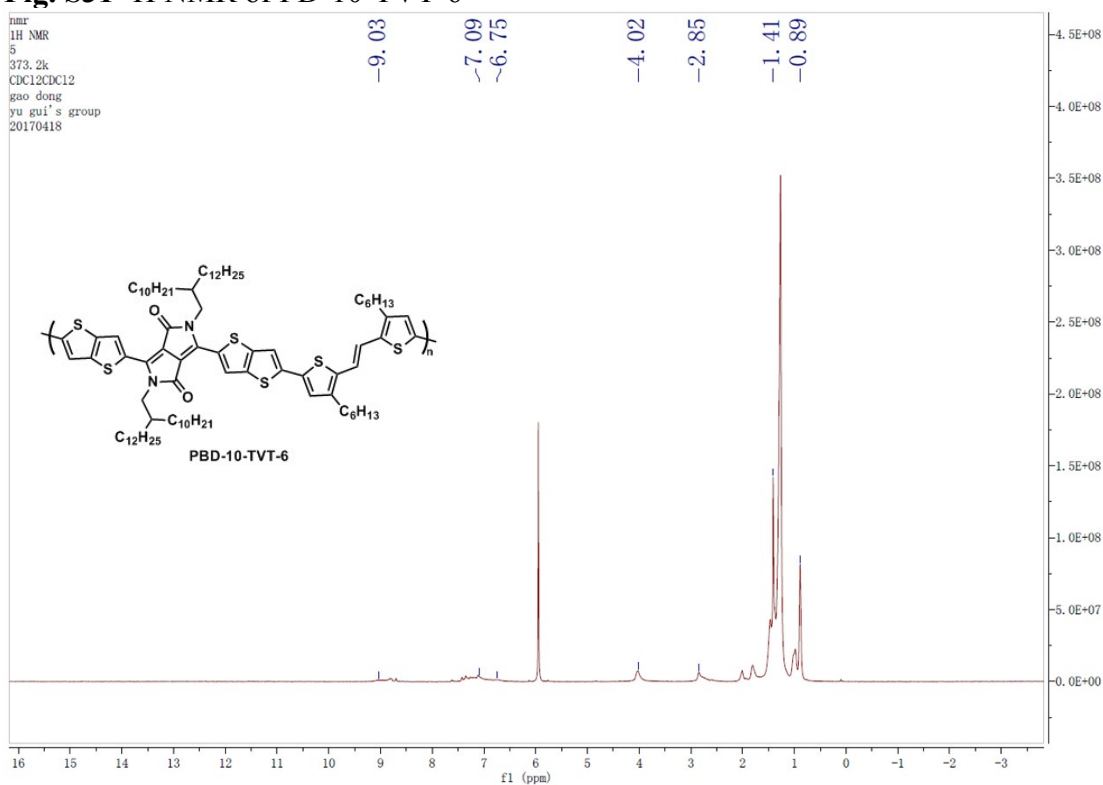
Fig. S31 ^{1}H NMR of PD-10-TVT-6

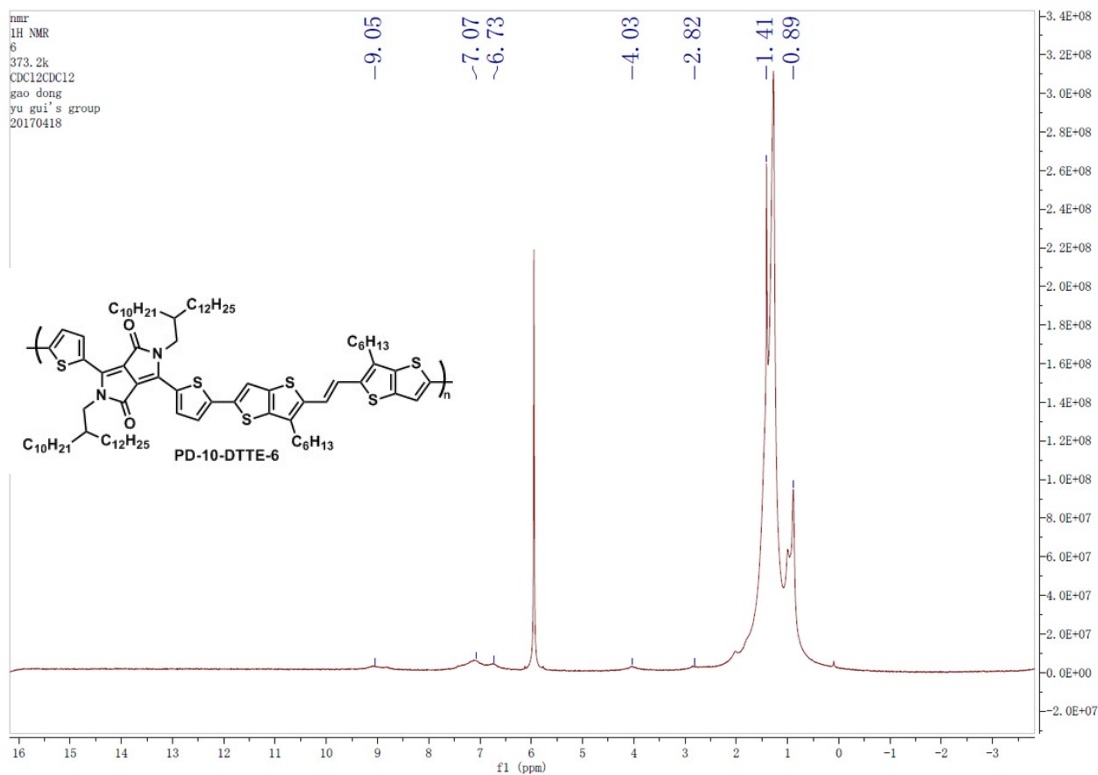**Fig. S32** ^{1}H NMR of PBD-10-TVT-6

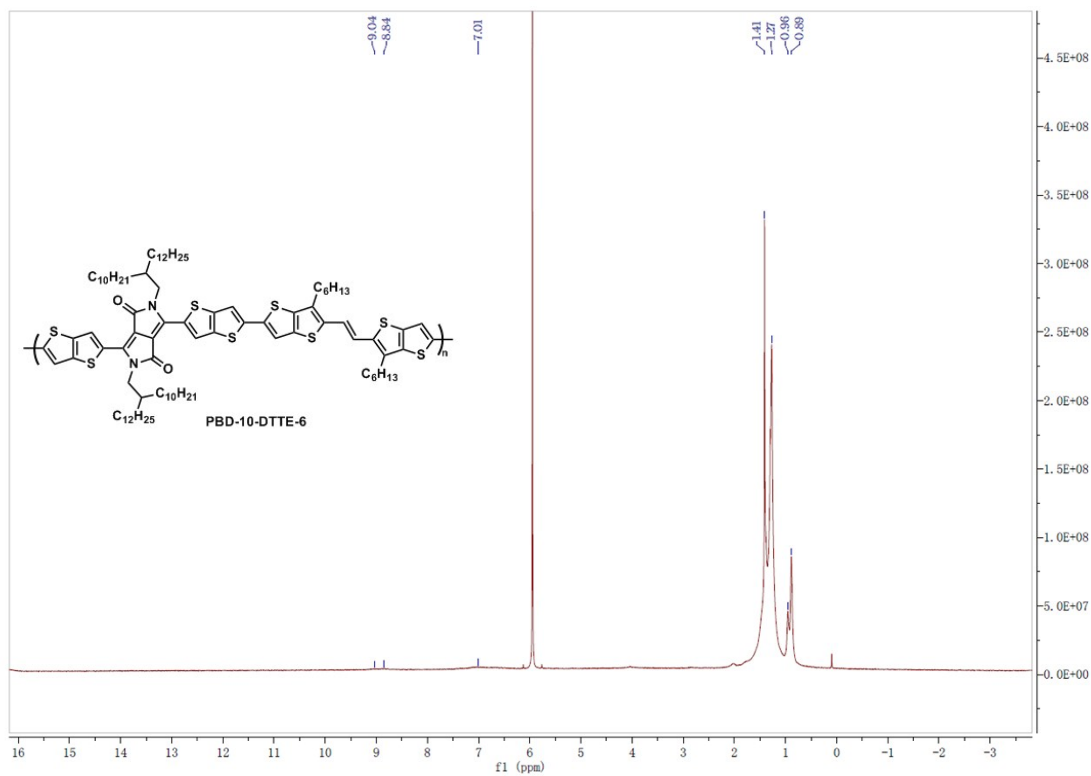**Fig. S33** ^{1}H NMR of PD-10-DTTE-6

Fig. S34 ^{1}H NMR of PBD-10-DTTE-6

References

1   M. He and F. Zhang, *J. Org. Chem.*, 2007, **72**, 442-451.
2   S. Tanaka, Y. Fukui, N. Nakagawa, K. Murakami, T. N. Murakami, N. Koumura and A. Mori, *Org. Lett.*, 2016, **18**, 650-653.
3   X. Liu, B. He, C. L. Anderson, J. Kang, T. Chen, J. Chen, S. Feng, L. Zhang, M. A. Kolaczkowski, S. J. Teat, M. A. Brady, C. Zhu, L. W. Wang, J. Chen and Y. Liu, *J. Am. Chem. Soc.*, 2017, **139**, 8355-8363.
4   L. Zhang, W. Shen, R. He, X. Liu, X. Tang, Y. Yang and M. Li, *Org. Electron.*, 2016, **32**, 134-144.
5   Z. Yi, Y. Jiang, L. Xu, C. Zhong, J. Yang, Q. Wang, J. Xiao, X. Liao, S. Wang, Y. Guo, W. Hu and Y. Liu, *Adv. Mater.*, 2018, **30**, 1801951.